Geomorphology 136 (2012) 114–131

Contents lists available at ScienceDirect

Geomorphology

journal homepage: www.elsevier.com/locate/geomorph

Review

Systematic morphometric characterization of volcanic edifices using digital elevation models

Pablo Grosse [a,*], Benjamin van Wyk de Vries [b], Pablo A. Euillades [c], Matthieu Kervyn [d], Iván A. Petrinovic [e]

[a] CONICET & Fundación Miguel Lillo, Miguel Lillo 251, (4000) San Miguel de Tucumán, Argentina
[b] Laboratoire Magmas et Volcans, Université Blaise Pascal, 5 Rue Kessler, 63038 Clermont-Ferrand, France
[c] Instituto CEDIAC, Universidad Nacional de Cuyo, Ciudad Universitaria, (5500) Mendoza, Argentina
[d] Department of Geography, Vrije Universiteit Brussel, Pleinlaan 2, 1050 Brussels, Belgium
[e] Centro de Investigaciones en Ciencias de la Tierra (CONICET), Av. Velez Sarsfield 1611, Ciudad Universitaria, X5016GCA, Córdoba, Argentina

ARTICLE INFO

Article history:
Received 31 March 2010
Received in revised form 1 June 2011
Accepted 1 June 2011
Available online 16 June 2011

Keywords:
Geomorphometry
Morphometric parameters
Digital elevation model
Volcanic edifice
Volcano morphometry

ABSTRACT

Quantitative characterization of the size and shape of volcanic edifices is an essential step towards the understanding of factors controlling volcano growth and morphology. The recent advent of digital elevation models (DEMs) with worldwide coverage offers the opportunity to systematically document the morphometry of all types of volcanoes using quantitative well-formalized methodologies. We present a methodology for the morphometric characterization of volcanic edifices. After reviewing previous studies on volcano morphometry and the various existing DEM sources, we describe an integrated procedure that uses a DEM and its derived products (slope, curvature) to extract a coherent set of morphometric parameters for a given volcanic edifice. Edifice boundaries are manually defined by searching for breaks in slope around the base. The parameters describe the overall size (basal and summit region area and widths, height, volume), planar shape (ellipticity and irregularity index of elevation contours), profile shape (height–width ratios) and slope of the edifice. Similar parameters for relatively large (depending on DEM spatial resolution) summit craters/calderas are also computed. Slope values and ellipticity and irregularity indexes are extracted for successive height intervals providing detailed information of volcano shape as a function of height. The number of secondary peaks is also estimated. The method is tested on thirteen composite volcanoes in Nicaragua using three DEM datasets (90 m SRTM, 30 m ASTER G-DEM and an 80 m topographic map-derived DEM) and the resulting parameters are evaluated in terms of boundary delineation and DEM source. Finally, the parameters obtained for the Nicaraguan volcanoes are discussed as an illustrative example of the type of data and information that can be extracted systematically for volcanoes worldwide.

1. Introduction

The shape and size of volcanoes are the result of complex evolutions involving the interaction of aggradational (effusion, deposition) and degradational (erosion, deformation) processes. The study of volcano morphology can give valuable insights into these processes and their underlying causes, i.e. tectonic/structural setting, magma composition and flux, eruptive style and climate (e.g., Cotton, 1944; Francis, 1993; Thouret, 1999; Davidson and De Silva, 2000). However, only limited effort has been dedicated so far to the characterization of volcano morphology in a systematic and comparable manner, as previously pointed out by Francis (1993) and Davidson and De Silva (2000).

With the advent of digital elevation models (DEMs) in the last couple of decades and their increasing accuracy, spatial resolution and availability, quantitative land-surface analysis (i.e. geomorphometry) has become increasingly widespread. Geomorphometry is now considered a scientific discipline in its own right (Pike, 1995; Hengl and Reuter, 2009) and geomorphometric analysis of DEMs is extensively applied in several scientific fields, particularly in geomorphology, hydrology, soil science, vegetation science and meteorology (e.g., Hengl and Reuter, 2009). The use of DEMs in volcanology has mainly focused on volcanic flow hazard modeling (e.g., Stevens et al., 2002; Huggel et al., 2008), volcano-tectonic analyses (e.g., Favalli et al., 2005; Lagmay and Valdivia, 2006) and in morphometric studies of specific volcano types or processes (see Section 2). The full potential offered by DEMs with worldwide coverage has yet to be exploited for systematic studies of volcano morphometry at a global scale. Research in this direction could make possible a comprehensive characterization and classification of the morphometry of volcanoes, and lead towards a better understanding of the factors controlling volcano morphology (e.g., Hone et al., 2007; Grosse et al., 2009; Karátson et al., 2010b).

We here describe a systematic methodology to extract quantitative morphometric parameters of volcanoes from DEMs, improving, extending and assessing the method originally presented by Grosse et al. (2009). Our aim is to define a set of morphometric parameters that comprehensively and objectively characterize the size and shape of most types of

* Corresponding author.
E-mail address: pablogrosse@yahoo.com (P. Grosse).

0169-555X/$ – see front matter © 2011 Elsevier B.V. All rights reserved.
doi:10.1016/j.geomorph.2011.06.001

volcanic edifices. We first review the existing literature on volcano morphometry and briefly describe the available DEM sources useful for volcanological studies. Next, we describe the methodology and the morphometric parameters, and then evaluate their performance as a function of DEM source and edifice boundary delineation. Finally, we present a case study that highlights the value of the morphometric parameters for volcanic edifice characterization and interpretation in terms of volcanological processes.

2. A brief review of studies on volcanic edifice morphometry

Before the advent of DEMs, studies on volcano morphometry were based on topographic maps, stereoscopic airphotos and/or field measurements. The earliest systematic morphometric studies were carried out on monogenetic cinder cones. Porter (1972) measured cone heights, basal diameters and crater diameters of cinder cones on Mauna Kea, Hawaii, establishing constant height/cone width and crater width/cone width ratios. Wood (1980a) confirmed and extended these ratios by measuring fresh cones from various regions, suggesting their validity for diverse tectonic settings and compositions. Similar measurements were carried out by Settle (1979), who compared the morphometry and spacing of cinder cones on the flanks of major volcanoes with those within flat-lying volcanic fields. Wood (1980b) and Dohrenwend et al. (1986) used the decrease in height/cone width ratio and in slope angle as proxies for cinder cone age and degradation. Hasenaka and Carmichael (1985) also measured heights and widths, and additionally calculated cone volumes and slopes using these measurements and considering the equation of a straight-sided truncated cone. Small shields have been measured in the same way (Hasenaka, 1994; Rossi, 1996). Another approach was that of Tibaldi (1995), who measured cone base and crater elongations, the location of depressions on the crater rim, and the alignment of cones, relating their azimuths with the geometry of the fracture feeding system and the regional tectonics. Some more recent studies of cinder cones also use topographic maps and field surveys, and apply similar parameters (e.g., Hooper and Sheridan, 1998; Carn, 2000).

The morphometry of composite or polygenetic volcanoes has received less attention than monogenetic cones, possibly because of their far greater complexity and thus greater difficulty in measuring and interpreting their shape. Early studies concentrated on some particular property, such as crater diameter (Simpson, 1967) or edifice size (Francis and Abbott, 1973), or on a particular volcanic region, such as Stoiber and Carr (1973), and later Carr (1984), who estimated the height and volume of the volcanoes of Central America, finding correlations with location along the volcanic front. In 1978, two publications presented systematic measurements of several morphometric parameters for composite volcanoes. Wood (1978) analyzed the morphometry of 26 historically active composite stratovolcanoes using the same parameters as for cinder cones. He showed that consistent linear variations existed between these parameters, suggesting geometrically uniform cone growth. Pike (1978) compiled morphometric data of 668 volcanoes, including both polygenetic and monogenetic volcanoes as well as thirteen Martian shields. He considered five morphometric parameters: height, width of flank, diameter and depth of summit depression, and circularity of crater (as well as six ratios). He also presented a 20-class volcano classification based on morphometry and composition. Pike and Clow (1981) later revised this classification and added volumetric values to each class.

More recently, with the advent and growing availability of DEMs, more sophisticated morphometric studies have been carried out. Using DEMs derived from topographic maps, Corazzato and Tibaldi (2006) investigated the connection of scoria cone morphology with structural setting on the flanks of Mt. Etna, whereas Dóniz et al. (2008) defined the most frequent scoria cone morphometry on Tenerife island. Favalli et al. (2009) used a high-resolution LiDAR DEM of Mt. Etna to measure the classical parameters for scoria cones, as well as volume and slopes, and refined the calculation method for cone height.

The slopes of oceanic shields have received particular interest. Mouginis-Mark et al. (1996) studied the slopes of the Galapagos shields using an airborne interferometric radar DEM, and introduced the analyses of slope as a function of height. Rowland and Garbeil (2000) extended this approach to Hawaii, Karthala and Piton de la Fournaise. Other recent studies focusing on slopes are those of Bleacher and Greeley (2008; Hawaii, using SRTM DEMs) and Michon and Saint-Ange (2008; Piton de la Fournaise, using a photogrammetric DEM).

Studies on the morphometry of stratovolcanoes using DEMs are few. Favalli et al. (2005) analyzed the morphometry of the Aeolian island volcanoes combining airborne photogrammetric DEMs with bathymetric data. Wright et al. (2006) introduced a dissection index of elevation contours as a way to quantify the shape of volcanoes. Grosse et al. (2009) analyzed the morphometry of arc volcanoes from Central America and the southern Central Andes, showing how morphometry can be used to interpret volcano growth trends. They used a former version of the method that we here extend and describe in detail (see Section 4). Karátson et al. (2010a) used DEM-based morphometry to reconstruct the shape and volume of an eroded stratovolcano. Karátson et al. (2010b) used SRTM DEMs to quantify the shape of nineteen circular and symmetrical stratovolcanoes, finding two types of upper flank profiles that can be related to different dominant eruptive styles.

Morphometric studies using DEMs of volcanoes from two contrasting settings have increased particularly in recent years, evidently because of the earlier lack of data: submarine volcanoes, or seamounts, and extraterrestrial volcanoes. Seamount morphometry has been studied with parameters similar to those for cinder cones (e.g., Smith, 1988, 1996; Rappaport et al., 1997; Clague et al., 2000; Stretch et al., 2006). Studies on the morphometry of extraterrestrial volcanoes range from the large Martian volcanoes (e.g., Plescia, 2004) to the small shields from Mars (e.g., Hauber et al., 2009) and Io (e.g., Schenk et al., 2004), and the pancake domes of Venus (e.g., Smith, 1996). Again, in these studies similar parameters are used.

In summary, several parameters and ratios have been used to quantitatively characterize volcanic constructs, but studies have generally focused on specific volcano types and on only a few parameters, whose choice depends on the volcano type (e.g., crater dimensions and height/width ratios for scoria cones; slopes for shields) or on the study objectives (e.g., height/width ratios and slopes in age studies; elongation and alignment in tectonic studies). No one has yet integrated a comprehensive set of parameters into a package that can be applied to most volcano types.

3. DEM sources for volcano morphometry

DEMs can be obtained from a variety of sources and generated in a variety of ways. Sources include ground surveys, existing topographic maps and remote sensing, which in turn can be either airborne or satellite-based. Methods include digitizing topographic maps, stereophotogrammetry, synthetic aperture radar (SAR) interferometry and laser scanning. Below and in Table 1 we present a brief overview of the available DEM sources that can be useful for studies on volcano morphometry.

The elevation data on topographic maps are obtained by ground surveying and/or airphoto stereoscopy. DEMs can be generated from existing topographic maps by manual or semi-automatic digitizing and scanning techniques (e.g., Carrara et al., 1997; Nelson et al., 2009). Resolution and accuracy of the created DEMs will vary depending on the original map quality and scale and on the quality of the DEM generation procedure (e.g., Favalli and Pareschi, 2004; Tarquini et al., 2007). The main disadvantage of this technique is that it is very laborious and time consuming. Some countries systematically produce nation-wide DEMs derived from topographic maps. They are in some cases free and publicly available (e.g., USA's 10 and 30 m resolution National Elevation Dataset,

Table 1
Summary of DEM sources and characteristics.
Modified from Kervyn et al. (2007) and Nelson et al. (2009).

Source	Method	Spatial resolution	Accuracy (vertical)	Scene size	Coverage	Cost	Distributor website
Topographic map	Digitizing/scanning	Variable	Variable	–	–	Variable	–
Airborne photography	Photogrammetry	<1 m	Very high, variable	Relatively small	–	~100–200€/km^2	–
Spaceborne optical sensors							
ASTER G-DEM	Photogrammetry	30 m	20 m	1°×1°	Near-global (83°N–83°S)	Free	www.gdem.aster.ersdac.or.jp
SPOT HRS	Photogrammetry	30 m	10 m	Variable	~2/3 of the Earth's land	2.30 €/km^2	www.spotimage.fr
High-resolution optical sensors	Photogrammetry	1–2 m	2–5 m	Relatively small	–	~5–40€/km^2	–
Airborne radar	Single-pass interferometry	10 m	1–2 m	–	–	–	–
Shuttle Radar Topography Mission							
SRTM C-band	Single-pass interferometry	30 and 90 m	5–10 m	1°×1° and 5°×5°	Near-global (60°N–57°S)	Free	Seamless.usgs.gov srtm.csi.cgiar.org
SRTM X-band	Single-pass interferometry	30 m	6 m	15′×15′	Idem but every other swath	400€/15′× 15′ tile	eoweb.dlr.de
Spaceborne synthetic aperture radar	Repeat-pass interferometry	~20 m	Variable	~100×100 km^2	–	>400€ per scene	–
Airborne LiDAR	Laser scanning	~1 m	0.1–1 m	Relatively small	–	~275–550€/km^2	–

NED), available on demand (e.g., Italy's 10 m TINITALY/01 DEM), or commercially available (e.g., France's 50 m resolution BD ALTI).

Photogrammetric DEMs are generated from optical sensors onboard either airborne or spaceborne platforms. Photogrammetry using aerial photographs is a standard technique (e.g., Lane et al., 2000). Resolution and accuracy will depend on the original quality and scale of the photographs but is generally very high (<1 m). Accuracy greatly increases with the use of ground control points (GCPs). However, availability of high quality aerial photographs with stereoscopic capabilities can be a major problem in many countries. Another drawback is the relatively small coverage of aerial photographs, making the DEM generating process painstaking for large areas.

Of the satellite-based photogrammetric DEM sources, the most cost effective solution for volcanological studies are provided by ASTER and SPOT 5. In both cases, DEMs are constructed from along-track stereo pairs. The ASTER Global Digital Elevation Model (G-DEM) is freely available since 2009 (http://www.gdem.aster.ersdac.or.jp). It has a 30 m spatial resolution, a 20 m vertical and 30 m horizontal accuracy, and covers the Earth between 83°N and 83°S. SPOT-HRS DEMs have a resolution of 30 m and accuracy of 10 m vertical and 15 m horizontal without GCPs. The stereo pairs are not available to the public and SPOT DEMs must be purchased (Spot Image, http://www.spotimage.fr). The coverage, as of February 2011, is 123 million km^2 (approximately 2/3 of the Earth's land surface) and the price for >3000 km^2 is 2.30€/km^2. Additionally, high resolution (~1–2 m) and accurate (2–5 m vertical accuracy) optical DEMs are constructed operationally using high-resolution optical sensors, such as those onboard the IKONOS and QuickBird satellites (e.g., Poon et al., 2005). They are used mainly for 3-D reconstruction of urban environments, but could be used to characterize small volcanic constructs. However, their high cost and relatively limited coverage constitute serious disadvantages.

Radar systems can generate DEMs by SAR interferometry (InSAR), a technique based on the phase difference between two recorded radar images or scenes (e.g., Ferretti et al., 2007). The procedure can be either single-pass interferometry (the two scenes are acquired at the same time) or repeat-pass interferometry (the two scenes are acquired at different times) and the systems can be on airborne or satellite platforms. Airborne radar systems use single pass interferometry, such as TOPSAR, which generates DEMs with 10 m spatial resolution and 1–2 m accuracy (Zebker et al., 1992).

The Shuttle Radar Topography Mission (SRTM) was carried out during 11 days of February 2000 onboard a NASA space shuttle (Rabus et al., 2003). It generated two single-pass interferometry DEM datasets from data acquired in two bands, C-band and X-band. The C-band DEM covers the entire land mass of the Earth between 60°N and 57°S and is freely available (USGS, http://seamless.usgs.gov; CGIAR-CSI, http://srtm.csi.cgiar.org), making it one of the most consistent, most complete and most used DEM in the world (e.g., Rabus et al., 2003; Nelson et al., 2009). Although the C-band data were acquired with a 1 arc second (~30 m) spatial resolution, the publicly available dataset has been degraded to a spatial resolution of 3 arc seconds (~90 m) for all areas outside the U.S.A. Accuracy estimates are 5–10 m vertical and 7–13 m horizontal, depending on location (Rodríguez et al., 2006). The 1 arc second resolution of the X-band DEM has been maintained, and it has an accuracy comparable to the C-Band. However, the X-band DEM covers only half the global area in alternating swaths and is not freely available; 15′×15′ tiles cost 400€ (German Aerospace Agency, http://eoweb.dlr.de).

Repeat-pass interferometric DEM construction using radar satellites, such as ERS-1/2, RADARSAT, ENVISAT and ALOS-PalSAR, is feasible, although relatively sophisticated and not implemented operationally at a global scale. Generated DEMs have resolutions of ~20 m and variable accuracies. Of particular interest are the DEMs that can be derived from ERS-1/2 tandem pairs, acquired during 1995 and 1996; coverage of this dataset includes almost the total global land surface (Duchossois et al., 1996).

Very high resolution (~1 m) and highly accurate (0.1–1 m) DEMs can be generated by using airborne Light Detection and Ranging (LiDAR) scanning techniques (e.g., Shan and Toth, 2008). Nelson et al. (2009) consider that LiDAR is 'the method of the future'. However, it is currently a very expensive method, requiring specifically designed flights and intensive elaboration of the raw data. LiDAR DEMs are particularly useful for studies of small structures, such as scoria cones (e.g., Favalli et al., 2009; Fornaciai et al., 2010) or lava flows (e.g., Ventura and Vilardo, 2008; Favalli et al., 2010).

Bathymetric DEMs of the seafloor are obtained by single or multibeam sonar systems; spatial resolutions are variable, generally between 10s and 100s of meters (e.g., Oehler et al., 2007). These types of DEMs are mostly constructed by research teams at specific locations and thus their availability and coverage is rather limited. Of the extraterrestrial planets, Mars has by far the best coverage. The Martian topography is almost completely covered by the freely available Mars Orbiter Laser Altimeter (MOLA) DEM, collected by the Mars Global Surveyor spacecraft (Zuber

et al., 1992; Smith et al., 2001); its spatial resolution is ~460 m. DEMs of other planets are restricted and of relatively poor resolution and quality.

4. A systematic methodology for the extraction of morphometric parameters of volcanic edifices

We here describe a method for obtaining morphometric parameters of volcanic edifices using DEMs. This method can be applied to any volcano that has a recognizable topographic construct (i.e. an edifice), such as stratovolcanoes, complex/compound volcanoes, shield volcanoes or monogenetic cones. It is thus not intended for volcanic landforms lacking an edifice such as calderas, maars, lava fields or fissure vents. The method itself is independent of edifice size, the constraint on size will be the resolution of the DEM used.

Fig. 1 is a flow chart showing the approach used for the computation of DEM-derived morphometric parameters of volcanic edifices. The initial steps of DEM preparation and topographic modeling (i.e. extraction of DEM-derived products) can be carried out using a variety of software packages, both free (e.g., GRASS, LandSerf, MicroDEM, SAGA) and commercial (e.g., ArcGIS, ENVI/IDL, ERDAS Imagine). Manual boundary delimitation based on DEM-derived products can also be performed with most of these software packages. For the computation of the morphometric parameters we have developed an IDL language code named MORVOLC. An initial version of this code was used and briefly described in Grosse et al. (2009). Here we describe in detail an improved and expanded version.

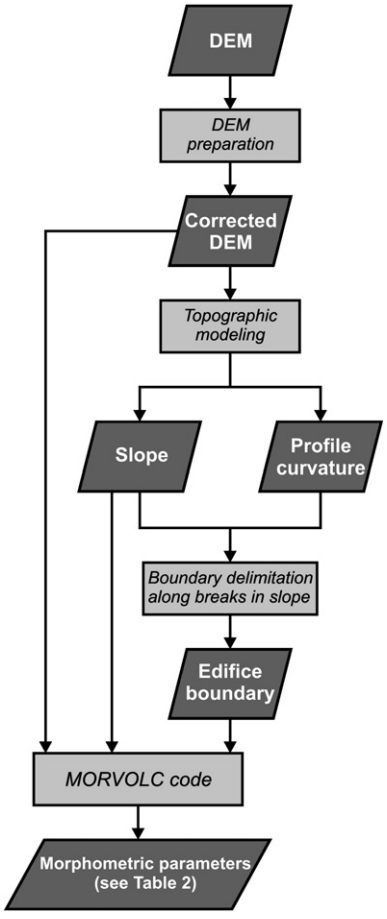

Fig. 1. Schematic flow chart of the implemented procedure for the extraction of morphometric parameters of volcanic edifices from DEMs.

4.1. DEM preparation and topographic modeling

DEMs usually contain errors that should be minimized prior to their use in morphometric analysis. Accordingly, preprocessing or preparation of DEMs is an important initial step. The type of preprocessing needed will depend on the type of errors, which in turn depends on the source and generation method of the DEM. Careful DEM inspection should be carried out and good knowledge of the DEM sources is recommended. A number of corrections are possible, such as noise filtering, outlier elimination, data void filling, ghost-lines and paddy terrace correction, etc. (see Reuter et al., 2009a, and references therein). Furthermore, morphometric analysis requires the DEM to be in a metric projection system; thus DEMs with latitude–longitude geographic coordinates (e.g., SRTM DEMs) must be projected.

From the corrected DEM, we derive slope and profile curvature maps. Both products are used for the next step of edifice boundary delimitation, and slope is also used in the computation of morphometric parameters. Several algorithms can be applied to calculate these topographic features, but the results correlate closely (e.g., Guth, 1995; Hodgson, 1998; Jones, 1998). We employ the formulation proposed by Wood (1996) and implemented in the ENVI/IDL software. Shaded relief images are also computed for visualization purposes.

4.2. Volcanic edifice boundary delimitation

In order to carry out morphometric computations, the spatial extent of each volcano of interest must be defined. This is a key step because it is a potential source of variability that will affect certain parameters (see Section 5).

Where a volcano 'starts' or 'ends' is an often difficult and subjective question. Volcanoes can merge with the surrounding landscape and volcanic products are often deposited at great distances from their source (e.g., fall deposits, lava flows along valleys). If the criterion selected for delineating a volcano is to consider all of its products, then topographic data are not sufficient and field- and/or remote-based geological data are needed. Even with this knowledge, it would be almost impossible to accurately account for the totality of products (e.g., volcanic products buried below other newer deposits, far reaching ash, etc.).

A more consistent approach, which we employ, is to consider only volcanic edifices as specific constructional landforms that are delimited by concave breaks in slope around their base; consequently, aprons and other far reaching products are disregarded. This criterion has the advantage of being based solely on topography, making it reasonably objective and enabling comparisons on a uniform basis. Furthermore, a separation of edifice and apron is not geologically arbitrary since it tends to correlate with the boundary between two main lithofacies associations (e.g., Davidson and De Silva, 2000): (1) the cone-building association, dominated by lava flows, pyroclastic flows, and products of flow reworking; and (2) the ring-plain association, dominated by fall tephra, debris fans, lahars and debris avalanche deposits. Examples of volcanoes where lithological contrasts at the edifice break in slope have been documented include Arenal (Borgia et al., 1988) and Mount Adams (Hildreth and Fierstein, 1997). However, this approach has the disadvantage that, because it considers only the edifice and not all of the volcanic products, it will lead to underestimates of the total volcano output and will reflect only the edifice size.

Many of the morphometric studies reviewed in Section 2 also consider breaks in slope as edifice limits (e.g., Pike, 1978; Plescia, 2004). In practice, edifice basal breaks in slope are sometimes obscured because they merge with aprons, neighboring volcanoes or other non volcanic deposits, and/or because of their own complex histories of vent migration, sector collapse, erosion, etc. Nevertheless, breaks in slope are generally readily identified, at least around most of the edifice base. In cases where a younger and smaller edifice is constructed on top of an older and larger edifice, two boundaries can be considered, one for each edifice, and

accordingly two sets of morphometric data can be computed. Also, for complex volcanoes made up of several coalescing edifices, morphometric parameters can be extracted for the whole complex massif and for each edifice separately.

There are a number of approaches to manual slope-break tracing usually using one or a combination of DEM-derived products (e.g., Smith and Clark, 2005). We carry out this procedure by jointly considering two DEM-derived products: profile curvature and slope (Fig. 2). Profile curvature is the rate of change of slope measured in a vertical plane oriented along the gradient line (e.g., Wood, 1996; Olaya, 2009). It thus directly maps breaks in slope, both convex (positive maxima) and concave (negative maxima). We also consider the actual slope values in order to favor slope breaks in lower gradient areas, typically found around the edifice base. Consequently, slope breaks in higher gradient areas, which are more common within the edifice, are penalized (Fig. 2).

In practice, we combine profile curvature and slope in a single data layer (Fig. 2) using the following equation, empirically derived after our own extensive testing:

$$\text{Boundary delineation layer} = \text{Profile curvature}_{\text{normalized}} * f + \text{Slope}_{\text{normalized}} * (1-f),$$

where

$$\text{Profile curvature}_{\text{normalized}} = (\text{Profile curvature}_{\text{n}} - \text{Profile curvature}_{\text{min}}) \div \textit{Profile curvature}_{\text{range}},$$

$$\text{Slope}_{\text{normalized}} = (\text{Slope}_{\text{n}} - \text{Slope}_{\text{min}})^2 / \left(\text{Slope}_{\text{range}}\right)^2$$

and f is a factor ranging from 0 to 1 that weighs each term and will depend on the topography of each particular case (we find that the visually more satisfying layers are generally obtained with values of f between 0.5 and 0.8). The generated layer is used to trace the boundary by manually searching for the best path around the edifice (i.e. the path along the minimum values of the generated data layer; Fig. 2). Manual delimitation has the inconvenience of user subjectivity and time consumption, but, as far as we know, we still lack effective automatic routines for volcanic edifice delimitation.

On volcanic islands, slope-break lines defining the edifice are often traceable above the shoreline, but in some cases, typically oceanic shields, slope-break lines are not clearly discerned, in which case the shoreline itself can be used as the edifice outline. However, the subaerial portion may sometimes represent only a small fraction of the total edifice volume. Full morphometric characterization of volcanic edifices that continue below sea level is feasible only if bathymetric data are available (e.g., Favalli et al., 2005; Oehler et al., 2007).

For volcanoes having relatively large summit calderas or craters (when compared with the DEM spatial resolution), we also manually trace the caldera/crater outlines in order to extract specific morphometric parameters of the caldera or crater. Defining these outlines is generally simpler because caldera/crater rims are clear topographic breaks, and thus manual delineation is quite straightforward.

4.3. Computation of morphometric parameters with the MORVOLC code

The inputs to the MORVOLC code are the corrected DEM, the slope map and the edifice boundary (obtained by the method described above or any other suitable one). Through a sequence of routines the program computes the set of morphometric parameters described in Section 4.4.

Several initial procedures are needed for the computation of the parameters. The edifice outline is used to generate a 3-D basal surface by computing a Triangular Irregular Network (TIN). The previous MORVOLC version generated this basal surface by fitting a first degree polynomial surface through the outline (Grosse et al., 2009), but we find the TIN surface to better fit the often irregular edifice boundaries; other algorithms could be used, such as kriging. If considering a summit caldera or crater, an equivalent 3-D crater surface is also computed.

Elevation contour lines are generated with the elevation interval chosen depending on the DEM resolution. As a rule of thumb, the interval should be approximately half the pixel size (e.g., a 50 m interval for the 90 m SRTM DEM).

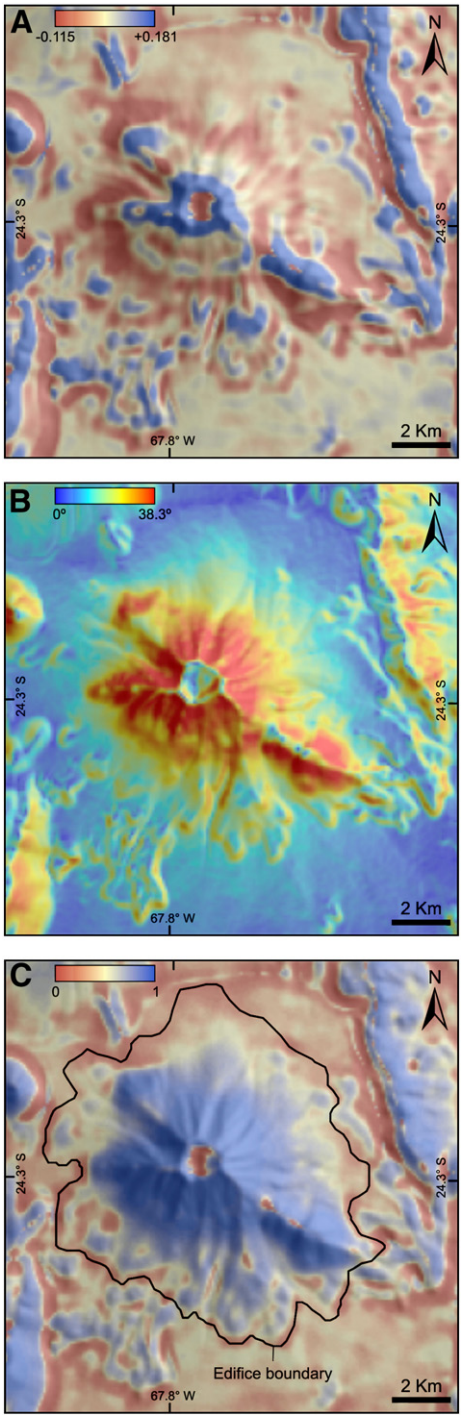

Fig. 2. Edifice boundary delineation procedure exemplified for Aracar volcano (Central Andes, Argentina) using the SRTM DEM; A) Profile curvature where positive maxima indicate maximum convexity and negative maxima indicates maximum concavity; B) Slope in degrees; C) Boundary delineation layer obtained from the combination of (A) and (B) (see equation in text) that is used to manually trace the edifice boundary along the path of minimum values.

Because most volcanic edifices show clear morphological differences between their flanks and their summit areas, a summit region is defined. The limit between the flank and summit regions is defined as the elevation where the edifice starts flattening out and is determined in two ways depending on the type of edifice. For simple edifices bounded by only one main contour per elevation value, the flank–summit limit will be the elevation at which the rate of slope decrease is greatest, i.e. where convexity is maximum. For more complex edifices bounded by more than one main contour per elevation value on their upper reaches, the flank–summit limit will be the elevation of the uppermost unique contour before the division into two or more main contours occurs. In both cases, the resulting summit region will depend on the chosen contour interval and thus on the DEM resolution, as well as on its accuracy, making this measure relatively inconsistent (see Section 5). The summit region outline is not equal to the summit caldera or crater rim, if present; the summit region will contain summit calderas/craters, covering a larger, and sometimes a much larger, area.

4.4. Morphometric parameters for characterizing volcanic edifices

In this section we describe the set of morphometric parameters that are computed with the MORVOLC code (Table 2). Although computation of other measures are possible (such as surface roughness, e.g., Grohmann et al., 2011, or circular symmetry, Karátson et al., 2010b),

Table 2
List of morphometric parameters for the characterization of volcanic edifices (expanded from Grosse et al., 2009).

Parameter (unit)	Description
Size parameters (*metric*)	
Basal area (A_B)	Planimetric area of the edifice outline
Basal width (W_B)	Average width of the edifice base calculated as SQRT(A_B/π)*2
Major basal axis (MAx_B)*	Length of the maximum base diameter passing through the base centroid
Minor basal axis (mAx_B)*	Length of the minimum base diameter passing through the base centroid
Summit area (A_S)	Planimetric area of the contour defined as the summit region
Summit width (W_S)	Average width of the summit region calculated as SQRT(A_S/π)*2
Major summit axis (MAx_S)*	Length of the maximum summit region diameter passing through the summit centroid
Minor summit axis (mAx_S)*	Length of the minimum summit region diameter passing through the summit centroid
Height (H)	Difference between the summit elevation and the elevation of the 3-D basal surface below the summit
Maximum height (H_{MAX})*	Difference between the summit elevation and the elevation of the lowest point of the edifice outline
Volume (V)	Volume enclosed between the DEM surface of the edifice and the 3-D basal surface
Maximum volume (V_{MAX})*	Volume enclosed between the DEM surface of the edifice and a horizontal base with elevation equal to the lowest edifice outline point
Shape parameters (*dimensionless*)	
Ellipticity index of flank contours [array] (*ei*)	Measure of the elongation of the main elevation contours that enclose the edifice (see text for equation)
Avg. ellipticity index of flank contours (ei_{AVG})	Mean average of all the *ei* values
Irregularity index of flank contours [array] (*ii*)	Measure of the complexity of the main elevation contours that enclose the edifice (see text for equation)
Avg. irregularity index of flank contours (ii_{AVG})	Mean average of all the *ii* values
Height/basal width ratio (H/W_B)	Measure of the overall steepness of the edifice
Summit width/basal width ratio (W_S/W_B)	Measure of the relative size of the summit region
Slope parameters (*degrees*)	
Avg. slope of the whole edifice (S_{TOT})	Mean and median average slopes of all the edifice
Avg. slope of the flank (S_{FL})	Mean and median average slopes of the edifice excluding the summit region
Avg. slope at height intervals [array] (S_H)	Mean and median average slopes of successive height intervals of the edifice
Maximum average slope (S_{MAX})	Mean and median average slopes of the height interval with the maximum average slope value
Height fraction of maximum avg. slope (HS_{MAX})*	Height fraction where the S_{MAX} is found
Orientation parameters (*degrees*)	
Azimuth of major basal axis (α_B)*	Azimuth (between 0° and 180°) of the direction of MAx_B
Azimuth of major summit axis (α_S)*	Azimuth (between 0° and 180°) of the direction of MAx_S
Azimuth of contours major axis [array] (α_H)*	Azimuths (between 0° and 180°) of the directions of the major axis of the main elevation contours
Peak count (*dimensionless*)	
Peak count of the edifice (PK_{TOT})*	Total number of peaks on the edifice calculated as the number of secondary elevation contours
Peak count of flank region (PK_{FL})*	Number of peaks on the edifice flanks calculated as the number of secondary elevation contours below the summit region
Peak count of summit region (PK_S)*	Number of peaks on the summit region calculated as the number of secondary elevation contours on the summit region
Summit caldera/crater parameters	
Crater area (A_C)*	Planimetric area of the crater outline
Crater width (W_C)*	Average width of the crater calculated as SQRT(A_C/π)*2
Major crater axis (MAx_C)*	Length of the maximum crater diameter passing through the crater centroid
Minor crater axis (mAx_C)*	Length of the minimum crater diameter passing through the crater centroid
Crater depth (D_C)*	Difference between the lowest crater elevation and the elevation of the 3-D crater surface above this point
Crater volume (V_C)*	Volume enclosed between the DEM surface bounded by the crater outline and the 3-D crater surface
Crater ellipticity (ei_C)*	Ellipticity index of the crater outline
Crater irregularity (ii_C)*	Irregularity index of the crater outline
Crater depth/crater width ratio (D_C/W_C)*	Measure of the overall profile shape of the crater
Azimuth of major crater axis (α_C)*	Azimuth (between 0° and 180°) of the direction of MAx_C
Avg. slope of the crater (S_C)*	Mean and median average slopes of the crater
Avg. crater slopes at height intervals [array] (S_{CH})*	Mean and median average slopes of successive height intervals within the crater
Crater width/basal width ratio (W_C/W_B)*	Measure of the relative width of the crater in relation to the edifice width
Crater depth/height ratio (D_C/H)*	Measure of the relative depth of the crater in relation to the edifice height

* New parameters with regards to those presented in Grosse et al. (2009).

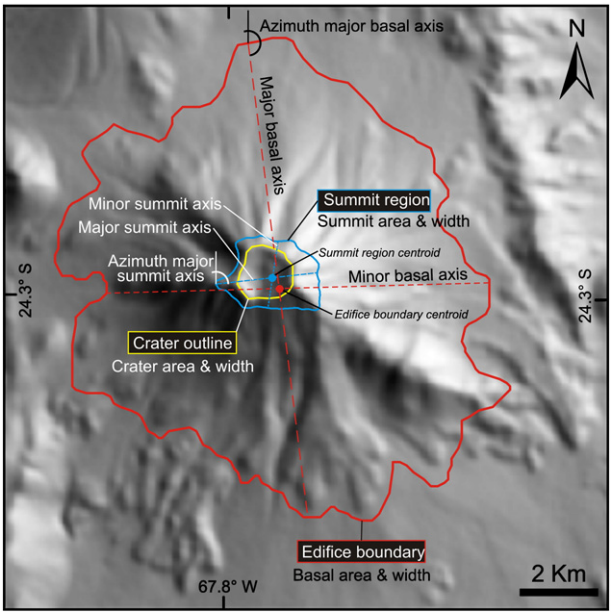

Fig. 3. SRTM DEM-derived shaded relief image of Aracar volcano (Central Andes, Argentina) showing basal, summit region and crater size and azimuth parameters.

our set of parameters quite thoroughly describes the size and shape of volcanic edifices, accounting for most of their first order variations.

4.4.1. Size parameters

The edifice boundary is used to directly calculate the planimetric area it encloses, i.e. the edifice *basal area* (A_B) (Fig. 3). Several linear measurements can also be obtained from the outline. In most morphometric studies (see Section 2), average width values are calculated as the arithmetic mean of the maximum and minimum widths of the outline. However, a more exact measure for the average *basal width* (W_B) of the edifice is the diameter of a circle with an area equal to that of the basal area (see also Favalli et al., 2009). Additionally, *major basal axis* (MAx_B) and *minor basal axis* (mAx_B) are the maximum and minimum straight lines contained within the outline and that pass through the outline centroid (Fig. 3). Equivalent parameters can be obtained from the summit region outline (Fig. 3): *summit area* (A_S), average *summit width* (W_S), *major summit axis* (MAx_S) and *minor summit axis* (mAx_S).

The absolute elevation values above sea level of a DEM will depend on its source, resolution and accuracy. The highest elevation value of the DEM within the edifice outline defines the location and elevation of its summit. This value is not a 'true' morphometric parameter of the edifice in the sense that it depends not only on the edifice but also on its location, and thus does not characterize the edifice morphometrically. On the other hand, the height of an edifice is an intrinsic parameter defined as the vertical distance from its base to its summit. This value is straightforward to measure for a horizontal base but not for an inclined or irregular base. We define *height* (H) of the edifice as the difference between the summit elevation and the calculated elevation of the reference basal surface in a position directly below the summit (Fig. 4). A useful additional measure is *maximum height* (H_{MAX}), which is the difference between the summit elevation and the lowest point of the edifice outline (Fig. 4).

Edifice or cone volumes have generally been estimated geometrically using the cone height and the base (and sometimes crater) width values, and considering idealized shapes such as a straight-sided cone, a straight-sided truncated cone, or a more complex exponential form (e.g., Francis, 1993). More recent studies have used DEMs to estimate edifice volumes more accurately, although calculations usually consider a horizontal base. A more precise approach is to calculate edifice volume using a 3-D reference basal surface (e.g., Favalli et al., 2009). The *volume* (V) will be the integrated sum of the difference between the DEM elevation and the basal surface elevation (Fig. 4). In other words, at each pixel, the square of the pixel size is multiplied by the height difference between the DEM and the basal surface, and then all the individual pixel volumes are added. As with height, it is also useful to estimate a *maximum volume* (V_{MAX}) considering a horizontal base (instead of the basal surface) with an elevation equal to the lowest outline elevation (Fig. 4). This method of estimating edifice volume depends exclusively on the selected outline, and hence on topography. It does not take into account possible geological complications such as sagging of the edifice (e.g., Concepción, Nicaragua; Borgia and van Wyk de Vries, 2003) or presence of older positive, or negative, topography beneath the edifice (e.g., Cordillera Central volcanoes, Costa Rica; Carr et al., 2007). In the case of sagging or of older negative topography, volume estimates will be lower than 'real', whereas in the case of older positive topography volume estimates will be larger. Another difficulty arises when the edifice coalesces with neighboring volcanoes or other positive topography. In this case a larger outline that includes all joined edifices can be used for the TIN surface generation in order to obtain more meaningful height and volume estimates.

4.4.2. Shape parameters

The shape of a volcanic edifice can be characterized by a series of parameters that refer to its plan and profile shape.

The plan shape of an edifice is defined by its bounding surface, which can be approximated by the set of elevation contours that enclose the edifice (Wright et al., 2006). Thus, edifice plan shape can be characterized by the shape of its elevation contours. With increasing DEM resolution, the number of well-constrained elevation contours will increase and consequently the detail in plan shape characterization will also increase.

The shape of complex contours, such as elevation contours, can be quantified by combinations of simple geometric measures (e.g., axial ratios, perimeter, area) into dimensionless indexes known as shape descriptors (e.g., elongation, circularity, compactness, etc., Davis, 1986). We derive two independent shape descriptor indexes that thoroughly describe the shape of elevation contours, the ellipticity index and the irregularity index (Figs. 5A–B and 6).

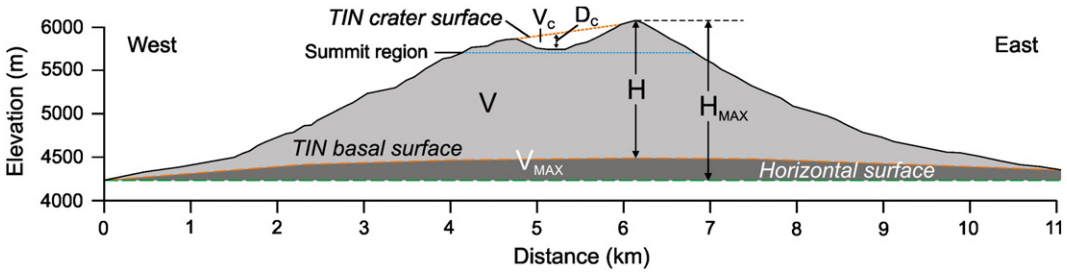

Fig. 4. SRTM DEM-derived West–East profile (no vertical exaggeration) of Aracar volcano (Central Andes, Argentina) illustrating the computed TIN basal and crater surfaces and the edifice height (H), maximum height (H_{MAX}), volume (V), maximum volume (V_{MAX}), crater depth (D_C) and crater volume (V_C) parameters.

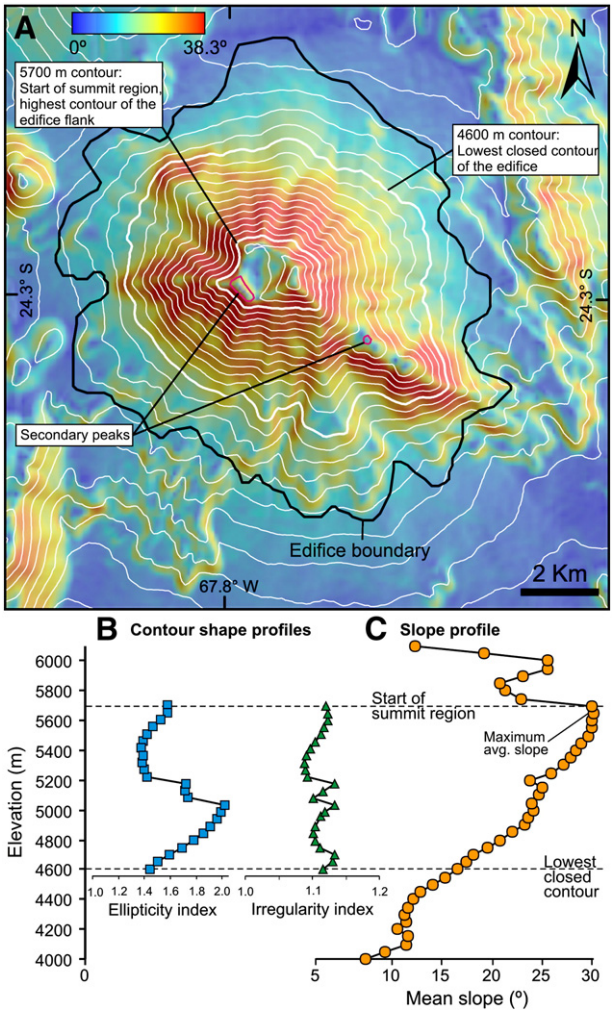

Fig. 5. A) SRTM DEM-derived slope map with 100 m interval elevation contours of Aracar volcano (Central Andes, Argentina); B) Ellipticity and irregularity indexes of the main closed contours on the edifice flank plotted as a function of elevation; C) Mean average slope plotted against elevation (in the plots elevation interval is 50 m).

The *ellipticity index* (*ei*) quantifies the elongation of each contour. It is a known shape descriptor that relates the length of the main axis of the contour with its area:

$$ei = \frac{\pi \times (L/2)^2}{A},$$

where *L* is the length of the major axis of the contour, and *A* is the area enclosed within the contour. The ellipticity index is equal to 1 for a circle and increases with increasing elongation. The average ellipticity index of all flank contours (ei_{AVG}) is an estimate of the plan-view elongation of the edifice. The ellipticity index is similar to the circularity index used by Pike (1978), but he only used it to describe the shape of crater rims, and to the circularity index defined by Karátson et al. (2010b). It is also similar to the base and crater ellipticities of cinder cones measured by Tibaldi (1995) and Corazzato and Tibaldi (2006), but they calculated ellipticity as the ratio between minimum and maximum diameters.

The *irregularity index* (*ii*) quantifies the irregularity or complexity of each contour. It is a modification, formerly described by Grosse et al. (2009), of the dissection index (*di*), which relates the perimeter with the area enclosed by the contour:

$$di = \frac{P}{2 \times A} \times \sqrt{A/\pi},$$

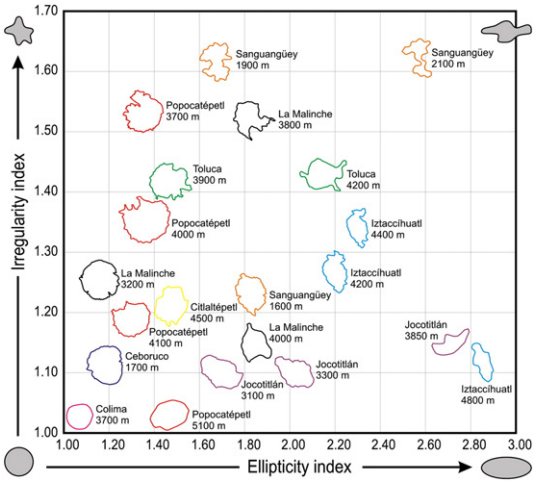

Fig. 6. Ellipticity index vs. irregularity index diagram of individual elevation contours (not to scale) of volcanic edifices from Mexico illustrating plan shape variations. See inset map of Fig. 7 for location of the volcanoes.

where *P* is the perimeter of the contour, and *A* is the area enclosed within the contour. Wright et al. (2006) used the dissection index to quantify the shape of elevation contours of volcanoes, showing its validity as a descriptor of volcano shape. However, and as pointed out by Wright et al. (2006), the dissection index is not only dependent on the complexity of the contour but also on its ellipticity. In order to obtain an index dependent only on contour complexity, Grosse et al. (2009) defined the irregularity index, which is equal to the dissection index of the contour minus the difference between the dissection index of an ellipse of equal ellipticity as the contour to that of a circle (i.e. 1):

$$ii = di_{contour} - \left(di_{ellipse} - 1\right), \quad \text{where } di_{ellipse} \text{ is the } di \text{ of an ellipse with a } ei_{ellipse} = ei_{contour}.$$

The irregularity index is equal to 1 for a circle and for any ellipse and increases with increasing complexity. The average irregularity index of

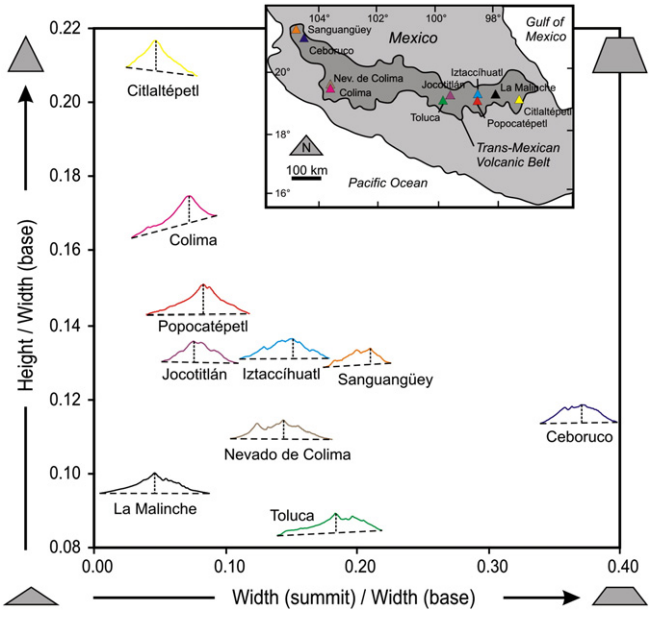

Fig. 7. Height/basal width ratio vs. summit width/basal width ratio of volcanic edifices from Mexico, illustrating varying profile shapes. Inset map shows location of the volcanoes.

all flank contours (ei_{AVG}) is an estimate of the plan-view irregularity of the edifice.

The ellipticity and irregularity indexes of successive elevation contours of an edifice define two independent curves that together summarize its plan shape and can be considered as a plan-shape 'fingerprint' (Fig. 5B). Only the main contours of the edifice flank are considered, up to and including the contour that defines the start of the summit region.

The profile shape of volcanoes has been commonly quantified using ratios of size parameters (mainly for monogenetic cones, see Section 2). Two ratios summarize the profile shape of a volcanic edifice as a whole, height/basal width and summit width/basal width. Other ratios which consider summit caldera or crater dimensions are presented in Section 4.4.6. The *height/basal width ratio* (H/W_B) is an estimate of the overall steepness of the edifice, whereas the *summit width/basal width ratio* (W_S/W_B) estimates how pointed or truncated the edifice is (Fig. 7). The W_S/W_B ratio assesses the relative importance of the summit region and, from our observations, usually roughly correlates with crater or caldera size, if present, and/or number of summit vents.

4.4.3. Slope parameters

The slope values of volcanic edifices have been widely used and considered indicative in classifications of volcano types (e.g., the classical separation of shields with gentle slopes and stratovolcanoes with steep slopes). Before the use of DEMs, slope averages were commonly estimated by simply assuming a straight-sided cone and using the cone height and width measures (see Section 2). From a DEM-derived slope map, several more sophisticated slope statistics

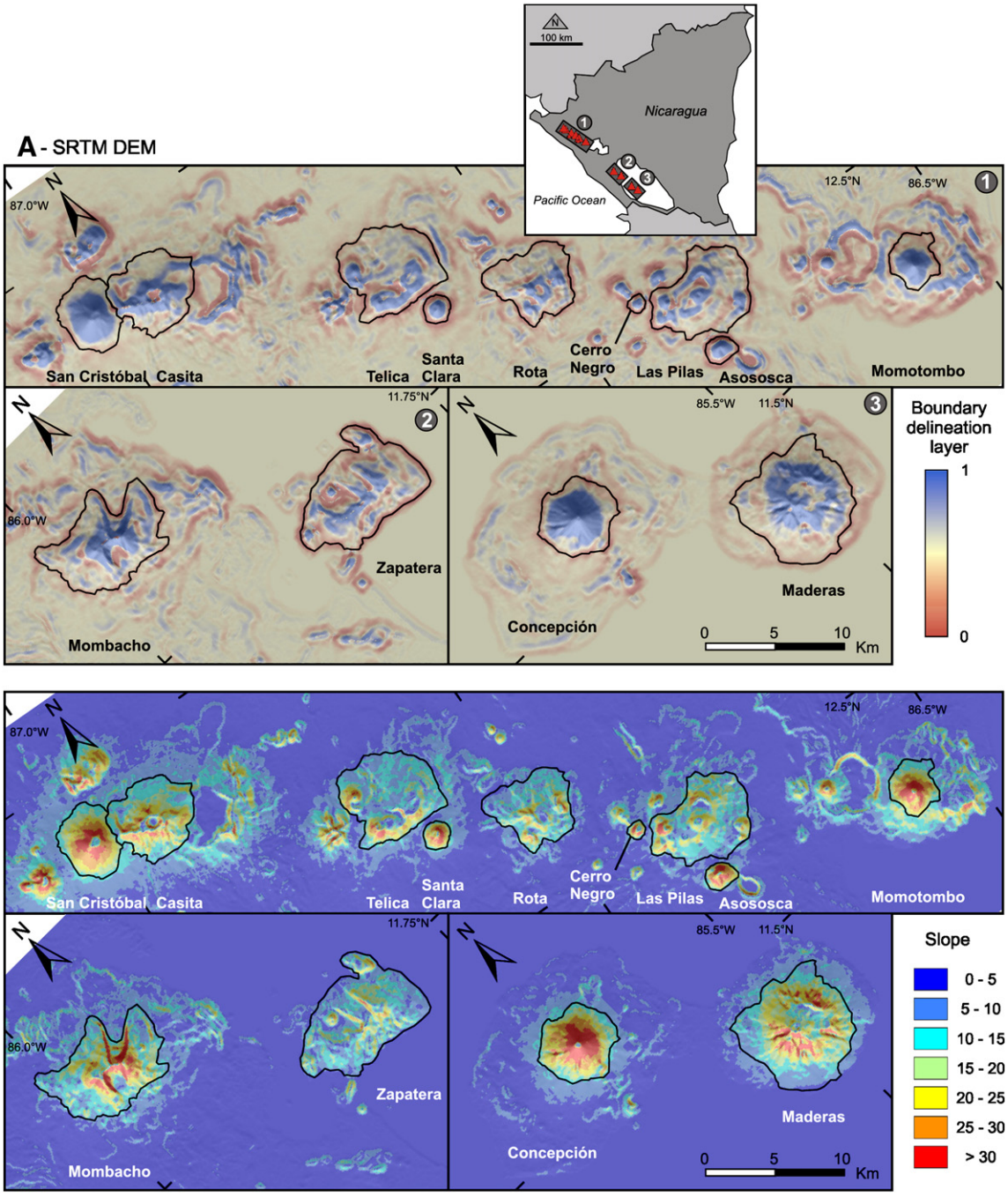

Fig. 8. DEM-derived images of Nicaraguan volcanoes obtained from (A) SRTM DEM, (B) ASTER G-DEM, (C) INETER TOPO DEM. For each DEM, the boundary delineation layer with edifice boundaries (top), and slope maps (bottom) are shown. Inset map in (A) shows location of the volcanoes.

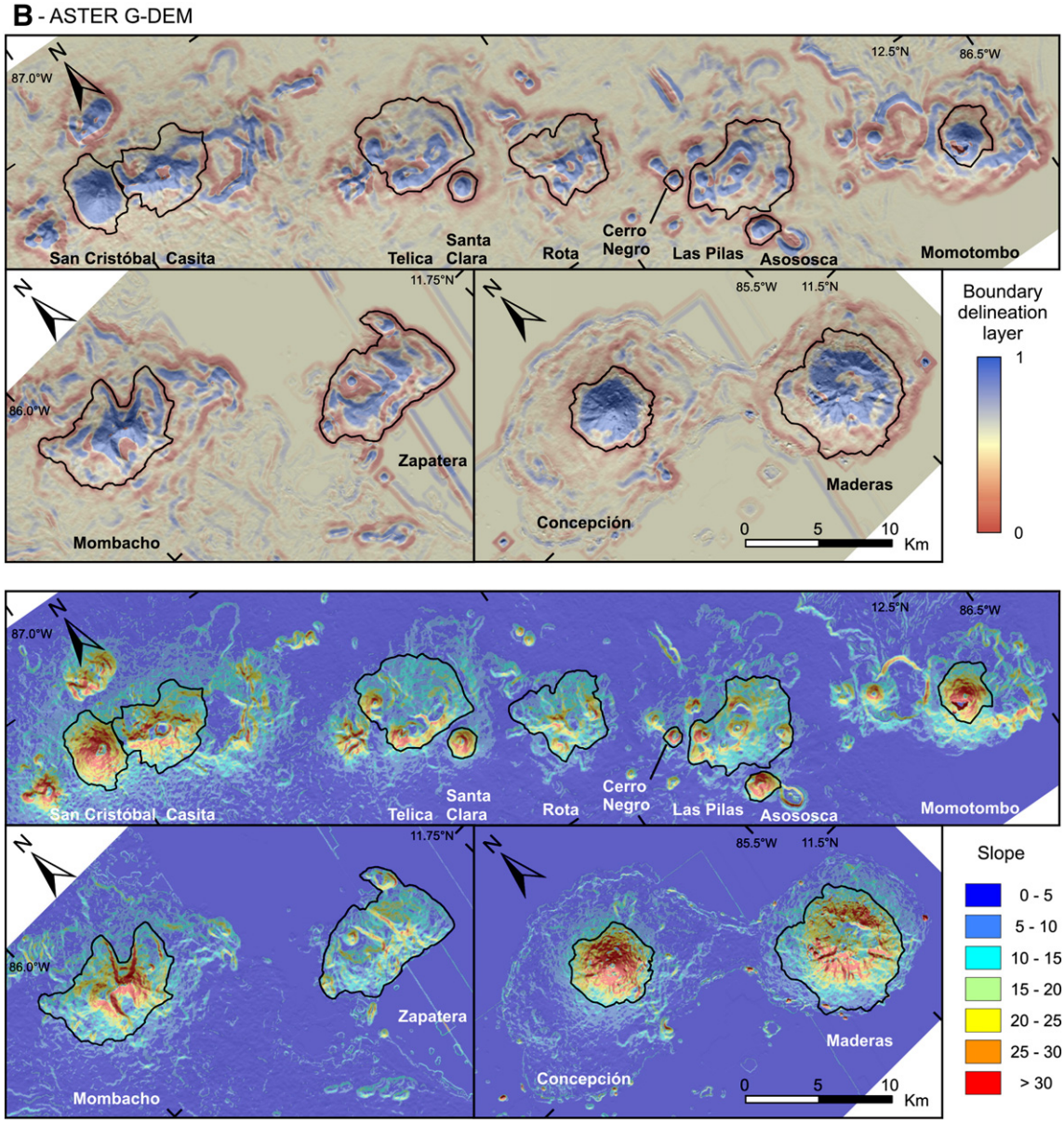

Fig. 8 (*continued*).

can be obtained. We extract both mean and median averages, as well as standard deviations. The *average slope of the whole edifice* (S_{TOT}) is probably not such a relevant parameter as it integrates the flank and summit regions. A more meaningful value is the *average flank slope* (S_{FL}), which better represents the average slopes of the edifice flanks, because it does not consider the summit region, which generally has very irregular gradients, especially if craters are present.

Average slopes at successive height intervals (S_H) define a curve that indicates how slope varies as a function of height (e.g., Mouginis-Mark et al., 1996; Rowland and Garbeil, 2000), and can be considered a profile-shape 'fingerprint' (Fig. 5C). The height interval with the highest average slope determines the *maximum average slope* (S_{MAX}) and the *height fraction of maximum average slope* (HS_{MAX}) (Fig. 5C). The H/W_B and W_S/W_B ratios, together with the slope vs. elevation data, summarize the volcano profile shape.

4.4.4. Orientation parameters

Orientation parameters related to some of the parameters described above are also computed. The *azimuths* of the major basal axis (α_B), the major summit axis (α_S) (Fig. 3), and of all the major axis of the main elevation contours (α_H) indicate the orientation of elongation of the edifice. Such measures of azimuth elongation have been used by Tibaldi (1995) and Corazzato and Tibaldi (2006) for cinder cones.

4.4.5. Peak count

The number of peaks contained within the edifice is an interesting measure because it can be related to the relief complexity and/or the number of secondary vents of the edifice. We estimate the number of peaks by counting the number of secondary elevation contours, both on the *flank* (PK_{FL}) and *summit* (PK_S) regions (Fig. 5A).

4.4.6. Summit caldera/crater parameters

For volcanoes with summit calderas or craters, the caldera/crater outline (Fig. 3) is used to obtain *crater area* (A_C) and *crater width* (W_C), as well as *major* and *minor crater axis* (MAx_C and mAx_C) and the *azimuth* of elongation (α_C). Similarly to the edifice height and volume calculations, a TIN surface of the caldera/crater outline will allow obtaining measures of *crater depth* (D_C) and *crater volume* (V_C) (Fig. 4). Attention should be drawn if there is a lake at the bottom of the caldera/crater as it will

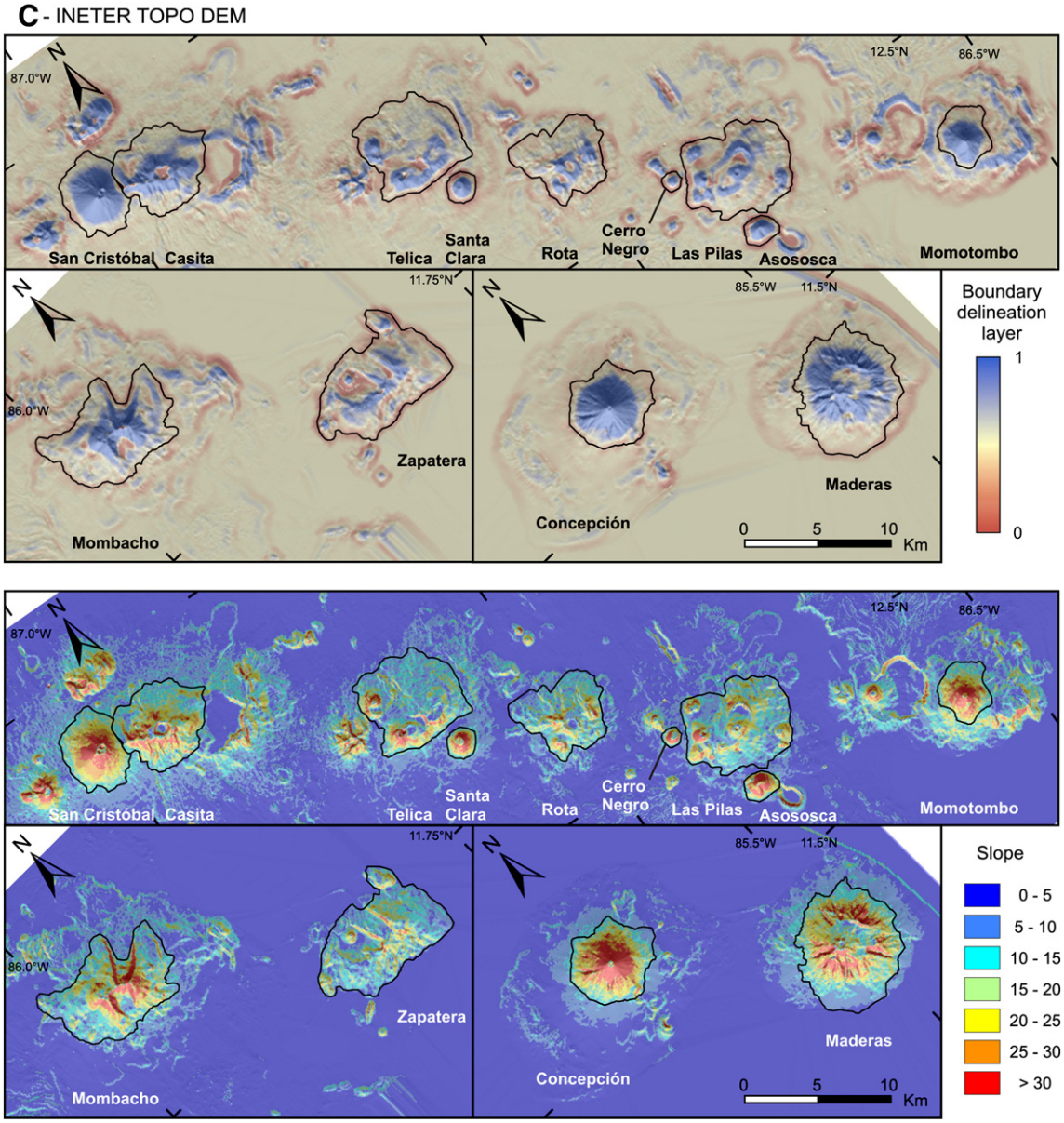

Fig. 8 (*continued*).

Table 3A
Morphometric parameter variation as a function of different edifice outlines for 13 Nicaraguan volcano edifices using the same SRTM DEM.

	Base area (km^2)				Height (m)			Volume (km^3)			H/W_B			W_S/W_B		
	Outline			%	Outline		%	Outline		%	Outline		%	Outline		%
	SRTM	ASTER	TOPO	*RSE*	SRTM	TOPO	*RSE*	SRTM	TOPO	*RSE*	SRTM	TOPO	*RSE*	SRTM	TOPO	*RSE*
Asososca	3.5	3.3	3.7	*3.2*	407	427	*2.4*	0.37	0.42	*6.0*	0.194	0.196	*0.6*	0.142	0.137	*1.8*
Casita	27.6	25.4	28.3	*3.2*	618	619	*0.1*	4.17	4.32	*1.8*	0.104	0.103	*0.6*	0.360	0.356	*0.6*
Cerro Negro	1.3	1.2	1.3	*3.1*	212	201	*2.7*	0.07	0.06	*9.0*	0.164	0.154	*3.1*	0.240	0.238	*0.4*
Concepción	24.0	23.5	25.4	*2.3*	1204	1226	*0.9*	6.73	6.92	*1.4*	0.218	0.216	*0.5*	0.072	0.070	*1.4*
Las Pilas	33.7	32.8	38.6	*5.1*	536	626	*7.7*	4.82	6.59	*15.5*	0.082	0.089	*4.3*	0.450	0.421	*3.4*
Maderas	53.2	52.2	47.2	*3.6*	1118	952	*8.0*	15.18	12.58	*9.4*	0.136	0.123	*5.1*	0.313	0.332	*3.0*
Mombacho	42.5	41.4	42.5	*0.9*	845	866	*1.2*	8.00	7.90	*0.6*	0.115	0.118	*1.2*	0.183	0.183	*0.0*
Momotombo	10.7	10.6	11.1	*1.5*	689	695	*0.4*	1.50	1.61	*3.5*	0.187	0.185	*0.6*	0.087	0.085	*1.1*
Rota	25.0	24.3	25.0	*1.0*	486	468	*1.9*	2.88	2.79	*1.7*	0.086	0.083	*1.9*	0.427	0.427	*0.0*
San Cristóbal	17.7	15.2	18.8	*6.2*	750	784	*2.2*	3.05	3.09	*0.6*	0.158	0.160	*0.6*	0.190	0.184	*1.6*
Santa Clara	3.2	3.2	3.5	*2.8*	393	401	*1.0*	0.36	0.38	*3.1*	0.194	0.191	*0.9*	0.179	0.173	*1.9*
Telica	36.0	34.9	36.6	*1.4*	442	454	*1.3*	4.43	5.07	*6.7*	0.065	0.066	*0.9*	0.451	0.447	*0.4*
Zapatera	49.5	45.9	46.1	*2.5*	562	550	*1.1*	6.44	6.08	*2.8*	0.071	0.072	*0.7*	0.129	0.134	*1.8*

underestimate the depth and volume values. The plan shape of the caldera/crater is summarized with the ellipticity and irregularity index of its outline (ei_C and ii_C), and its profile shape with the *crater depth/crater width ratio* (D_C/W_C). Statistics of the inner slopes of the caldera/crater are also computed (S_C, S_{CH}). Additionally, the size of the caldera/crater in relation to the edifice size is estimated with the *crater width/basal width* (W_C/W_B) and *crater depth/height* (D_C/H) ratios.

5. Method evaluation as a function of DEM source and edifice boundary

We here evaluate the methodology in terms of DEM source and edifice boundary selection by examining the variation of the morphometric parameters obtained from an analysis of thirteen volcanoes in Nicaragua using three DEMs (Fig. 8): the 90 m SRTM DEM, the 30 m ASTER G-DEM and an 80 m resolution DEM derived from digitizing topographic maps (TOPO DEM for short). The publicly available and near-global SRTM and ASTER DEMs are two of the most widely used DEM datasets and represent two of the most common DEM-generating methods, radar interferometry and optical photogrammetry. The TOPO DEM is a mid-resolution and mid-accuracy topographic map-derived DEM typical of many national geographical surveys. Thus, assessment of the methodology using these three DEMs provides a broad test whose validity can be extrapolated to other DEMs with similar resolution and accuracy. Furthermore, Nicaragua contains volcanoes with a great variety of morphologies, making it an ideal location for the evaluation of the method.

The SRTM DEM dataset from CGIAR-CSI was used (Jarvis et al., 2008). This version of the SRTM DEM is seamless as voids have been filled by interpolation techniques (Reuter et al., 2007). On the contrary, the ASTER G-DEMs usually have numerous errors and artifacts (e.g., Reuter et al., 2009b); the downloaded ASTER G-DEM contains clearly visible artificial 'pits' and 'hills'. A notable example of an artificial 'hole' occurs on the southern flank of Momotombo volcano (Fig. 8B); we have analyzed this volcano using both the raw ASTER G-DEM and a corrected hole-filled version in order to compare the resulting parameters. The

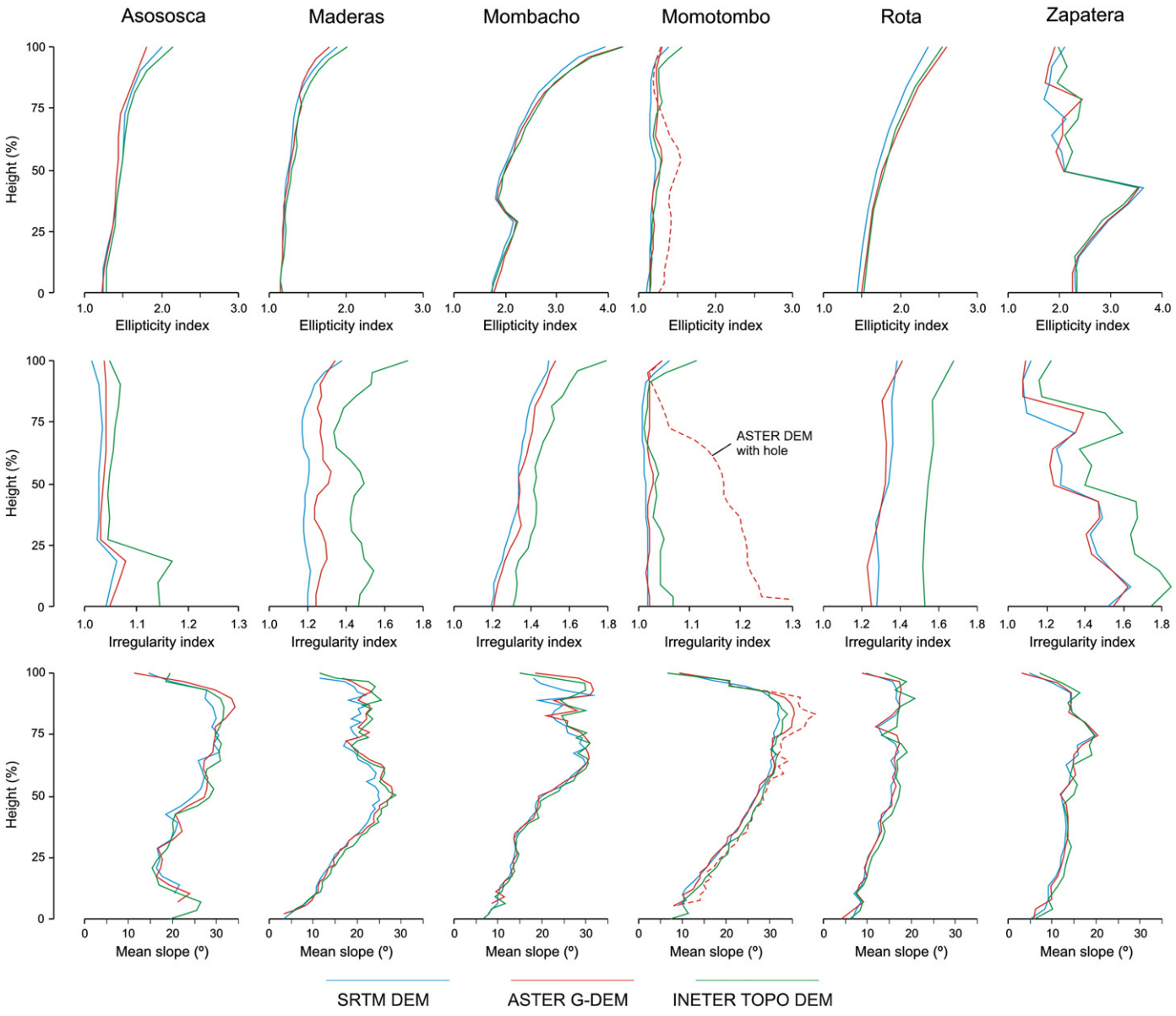

Fig. 9. Ellipticity index, irregularity index and mean slope profiles plotted as a function of height (%), obtained from the SRTM, ASTER and TOPO DEMs, for six Nicaraguan volcano edifices.

TOPO DEM was made by the Instituto Nicaragüense de Estudios Territoriales (INETER) by digitizing 1:50,000 scale topographic maps with elevation contours every 20 m; the original elevation data derives from ground surveys and photogrammetry.

For each of the DEMs we derived slope and profile curvature raster images and computed the combined layer for the manual boundary delimitation of the volcanic edifices. The boundary layers and the resulting outlines are shown in Fig. 8. We then computed the morphometric parameters using the different outlines and DEMs. Table 3 and Fig. 9 summarize the obtained values and their variability. Table 3A shows parameter values and variability in terms of different edifice outlines, whereas Table 3B and Fig. 9 shows parameter values and variability in terms of the different DEM sources. We use the relative standard error (RSE), expressed as a percentage, to estimate data variability.

The edifice boundaries obtained from the three DEMs vary in size by less than ±1% RSE in area to up to a maximum of ±6.2% RSE in area (±3.1% RSE in average width) for the San Cristóbal outlines. The greater differences (e.g., the larger TOPO outlines of Las Pilas and Maderas; the smaller ASTER outline of San Cristóbal; Fig. 8) are the result of having taken different paths when tracing the boundaries, a problem that occurs when more than one slope break line is present; for example, in the case of Las Pilas, the TOPO outline includes the Cabeza de Vaca cone to the North whereas the SRTM and ASTER outlines do not (Fig. 8). The average of the variations of all outlines is ±3% in area (±1.5% in width). This value can be considered as an approximate uncertainty estimation for any given outline drawn using our method.

The edifice outlines will not only directly affect the basal size parameters, but will also affect the height and volume estimates because the outlines are used to compute the 3-D basal surfaces which are in turn used to calculate heights and volumes. However, these parameters will also depend on the DEM itself. In order to evaluate separately the variability caused by outline size and DEM source, we have calculated parameters using two different outlines (the SRTM and TOPO outlines) on the same SRTM DEM (Table 3A), and then using the same SRTM outline on the three different DEMs (Table 3B).

The effect of different edifice outlines on height and volume will depend in each particular case on the topography of the region that is included in one outline and not in the other; e.g., if this region is flat, even large boundary differences will have little effect on the resulting height, whereas if this region is steep the resulting heights and volumes may vary considerably. Similarly, if this region contains positive topography (e.g., a parasitic cone) then the resulting heights may suffer little variation whereas volumes will vary much more. In general, height, volume and the H/W_B ratio correlate positively with outline size (Table 3A). Height varies at a rate similar to base area variation, whereas volume varies at approximately twice the rate, because it depends on the product of the basal area and height. On the other hand, the H/W_B ratio is the quotient of these measures and thus varies only at half the rate of base area variation. Because the summit width does not depend on the edifice outline size, the W_S/W_B ratio is in direct inverse relation to the base width, and thus also varies at half the rate of base area variation. Thus in general, the average outline uncertainty of ±3% in area (±1.5% in width) translates into height uncertainties of around ±3%, volume uncertainties of around ±6%, and H/W_B and W_S/W_B ratio uncertainties of around ±1.5%. For example, given an edifice with a base area of 50 km^2, a height of 1000 m and a volume of 10 km^3, the uncertainties related to the uncertainty of the outline delineation can be estimated at ±1.5 km^2 in base area (±120 m in base width), ±30 m in height, ±0.6 km^3 in volume and ±0.002 in the H/W_B ratio.

Considering the same outline for the three DEMs (Table 3B), height varies from ±0.4 to ±2.3% RSE, with an average of ±1.4%. Most

Table 3B
Morphometric parameter variation as a function of DEM source for 13 Nicaraguan volcano edifices using the same outline.

	Height (m)				Volume (km^3)				H/W_B			
	DEM			%RSE	DEM			%RSE	DEM			%RSE
	SRTM	ASTER	TOPO		SRTM	ASTER	TOPO		SRTM	ASTER	TOPO	
Asososca	407	421	440	2.3	0.37	0.39	0.38	1.2	0.194	0.201	0.210	2.3
Casita	618	613	647	1.7	4.17	4.17	4.29	0.9	0.104	0.103	0.109	1.7
Cerro Negro	212	218	228	2.2	0.071	0.074	0.085	5.4	0.164	0.169	0.177	2.2
Concepción	1204	1221	1245	1.0	6.73	6.84	6.84	0.5	0.218	0.221	0.225	1.0
Las Pilas	536	545	536	0.6	4.82	5.05	4.93	1.4	0.082	0.083	0.082	0.6
Maderas	1118	1108	1132	0.6	15.18	15.47	14.75	1.4	0.136	0.135	0.137	0.6
Mombacho	845	863	881	1.2	8.00	8.07	7.83	0.9	0.115	0.117	0.120	1.2
Momotombo	689	708	714	1.1	1.50	1.51	1.54	0.7	0.187	0.192	0.194	1.1
Rota	486	479	501	1.3	2.88	2.97	2.99	1.1	0.086	0.085	0.089	1.3
San Cristóbal	750	774	805	2.1	3.05	3.13	3.21	1.4	0.158	0.163	0.170	2.1
Santa Clara	393	393	397	0.4	0.36	0.36	0.35	0.9	0.194	0.194	0.196	0.4
Telica	442	439	461	1.5	4.43	4.55	4.41	1.0	0.065	0.065	0.068	1.5
Zapatera	562	532	574	2.2	6.44	6.21	6.30	1.1	0.071	0.067	0.072	2.2
	W_S/W_B				Peak count				Mean slope			
	DEM			%RSE	DEM			%RSE	DEM			%RSE
	SRTM	ASTER	TOPO		SRTM	ASTER	TOPO		SRTM	ASTER	TOPO	
Asososca	0142	0.136	0.110	7.6	1	1	1	0.0	23.5	24.0	24.3	1.0
Casita	0.360	0.366	0.350	1.3	4	3	5	14.4	16.9	17.3	17.9	1.8
Cerro Negro	0.240	0.239	0.209	4.5	1	1	1	0.0	18.6	19.1	19.3	1.1
Concepción	0.072	0.084	0.110	12.6	1	4	3	33.1	22.6	23.6	23.2	1.2
Las Pilas	0.450	0.451	0.431	1.5	8	9	10	6.4	13.7	14.2	14.4	1.4
Maderas	0.313	0.328	0.303	2.3	5	14	8	29.4	16.6	17.8	17.6	2.1
Mombacho	0.183	0.169	0.175	2.3	4	4	4	0.0	16.4	16.8	17.0	1.1
Momotombo	0.087	0.101	0.069	10.7	1	1	1	0.0	21.5	21.5	22.0	0.8
Rota	0.427	0.395	0.408	2.2	5	4	7	16.5	12.7	13.0	13.7	2.1
San Cristóbal	0.190	0.214	0.199	3.5	1	1	1	0.0	21.8	22.3	22.5	0.9
Santa Clara	0.179	0.181	0.158	4.2	1	1	1	0.0	22.3	22.6	22.8	0.7
Telica	0.451	0.430	0.453	1.6	5	5	8	16.7	12.6	13.1	13.5	2.1
Zapatera	0.129	0.135	0.112	5.3	13	19	17	10.8	11.0	11.3	11.4	1.0

variation is caused by the greater heights obtained from the TOPO DEM, probably because in its construction summit point elevations were taken into account, as opposed to the other two DEMs where summits are smoothed out. The height variations considering only the SRTM and ASTER DEMs are below ±1.6% RSE (±0.9% average) with the exception of Zapatera, which gives an anomalously low height on the ASTER DEM. The H/W_B ratio will have the same variations as height when considering the same outline. Excluding Cerro Negro, volume varies from ±0.5 to ±1.4% RSE, with an average of ±1.0%. Cerro Negro's small size (volume<0.1 km^3) probably becomes an issue at the DEM's resolutions. The SRTM volumes are generally lower than the ASTER volumes, because of the SRTM's lower resolution and greater smoothing. The ASTER volume of Momotombo increases from 1.46 km^3 to 1.51 km^3 if the artificial 'hole' on its flank is filled. The W_S/W_B ratio will depend on the contour that defines the summit region. The width of the summit region (and consequently the W_S/W_B ratio) varies from ±1.3 to ±12.6% RSE, with an average of ±4.6%. The greater variations are found on the volcanoes with smaller summits (e.g., Concepción, Momotombo), where even small differences in the size of the summit region contour will be enhanced. Peak count will depend on the chosen elevation interval of contours and on the roughness of the DEM. For the same interval, the SRTM DEM gives fewer peaks because of its lower resolution and greater smoothing, whereas the ASTER and TOPO DEMs give similar counts. The greater number of peaks on the ASTER DEMs can be related not only to its higher resolution but also to a noise problem that can create small artificial 'hills' (Kervyn et al., 2008). The smoothing of the SRTM DEM is also evident considering the mean slopes of the whole edifices. The SRTM DEM gives lower average slope values and also lower standard deviations. ASTER and TOPO average slopes and standard deviations are similar.

Fig. 9 shows *ei*, *ii* and slope profiles of selected edifices obtained from the three DEMs. A lack or small number of contours can be a problem for small edifices (e.g., Cerro Negro), for complex edifices with a large summit region that starts relatively low (e.g., Las Pilas, Telica) and for edifices that coalesce with others (e.g., Casita). For these types of edifices, only a few *ei* and *ii* values can be obtained and they are thus of limited use as shape descriptors. The profiles have similar overall shapes, with similar inflections, but the absolute values can vary. The *ii* profiles vary the most, whereas the *ei* and slope profiles are more consistent between DEMs. The

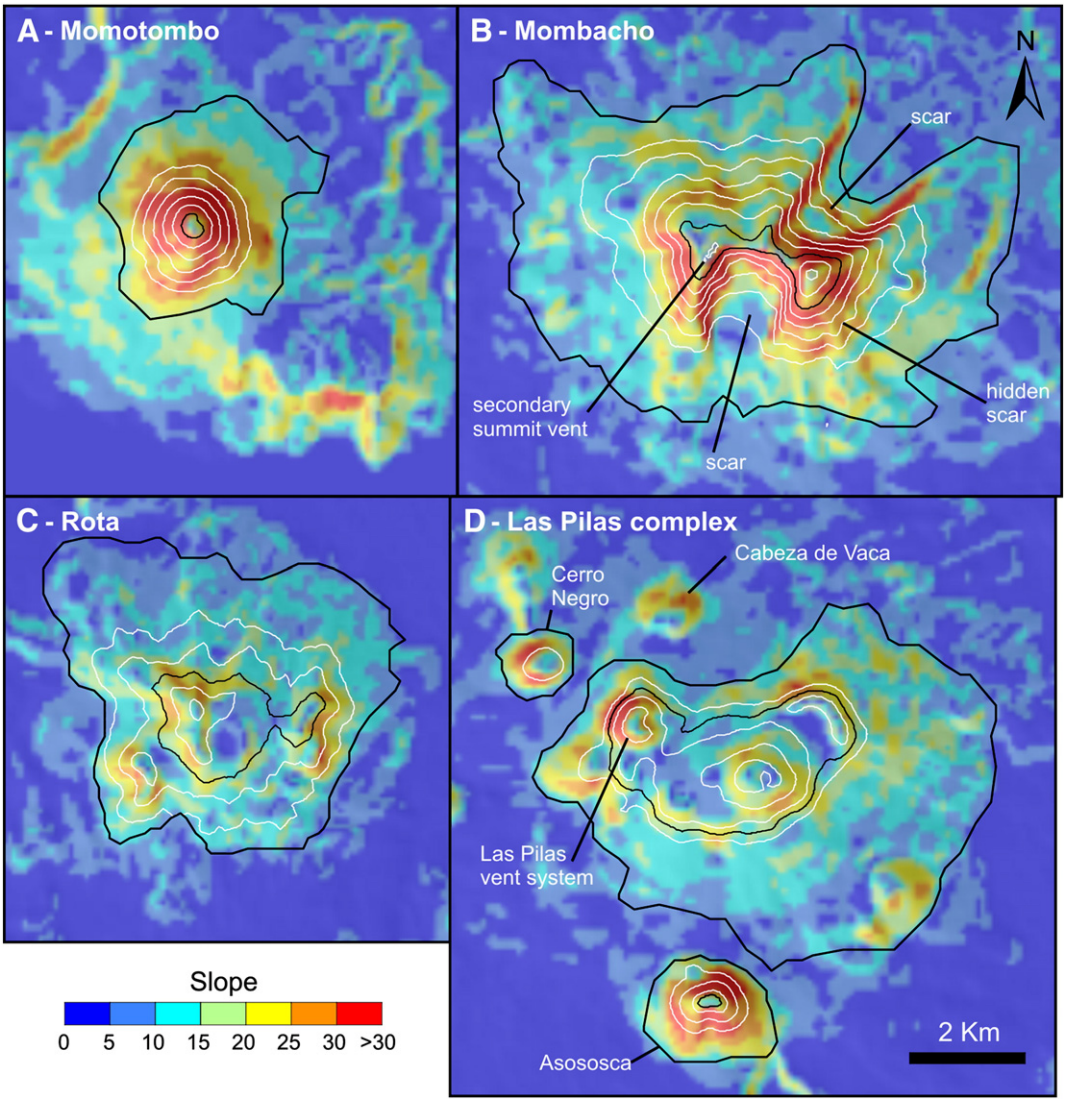

Fig. 10. SRTM DEM-derived slope maps of representative Nicaraguan volcanoes. Edifice boundaries and summit regions are shown in black and 100 m-interval elevation contours within the edifices in white. A) Momotombo is a small conical edifice that has grown rapidly, as seen by the smooth and steep conical shape; B) Mombacho is a sub-conical edifice; it has developed more than one vent, a recent secondary vent has added a westward extension to the main edifice; collapse scars are shown, two are still clear features, but one has been filled in C) Rota is a small massif showing a rough irregular surface caused by tectonic faulting and erosion. D) Las Pilas is a complex massif with a smooth surface, due to its frequent activity, but is very elliptical; small associated cones, such as the Las Pilas vent system, Cerro Negro, Asososca and Cabeza de Vaca are indicated. Cerro Negro, while small, already has an elliptical shape and more than one vent.

SRTM profiles generally have lower values, in agreement with the SRTM lower resolution and greater smoothing (e.g., Wright et al., 2006), the ASTER profiles are intermediate and the TOPO profiles have larger values, and sometimes much larger in the case of the *ii*. ASTER DEM errors will have a strong effect on the resulting profiles, as illustrated by the 'hole' on Momotombo (Fig. 9). The high irregularity of the TOPO DEM contours are possibly related to the photogrammetric techniques and/or interpolation method that were used in its construction.

6. Case study: Nicaragua composite volcanoes

In the following, we discuss the morphometric data obtained using the 90 m SRTM DEM for the thirteen Nicaraguan volcanoes evaluated in the previous section, as an illustrative example that shows the relevance of some of the parameters for the morphometric characterization of volcanic edifices and for the interpretation of several volcanological processes. The different types of edifice shapes are briefly characterized, and four edifices are described in more detail to highlight the different morphometries: Momotombo, Mombacho, Rota and the Las Pilas complex (Fig. 10).

Three main types of edifice shapes can be recognized based purely on the morphometric data (Figs. 11 and 12): (1) regular conical edifices; (2) composite or compound edifices with semi- or sub-conical shapes (for simplicity we use here the term 'sub-conical' for these edifices, following the classification of Grosse et al., 2009); and (3) complex centers or massifs with irregular shapes. The very small Cerro Negro, Santa Clara and Asososca cones can be considered a sub-class of small composite cones or large scoria cones within the conical-type edifices (see McKnight and Williams, 1997, for a discussion on the nature of Cerro Negro). With the exception of these small cones and Casita, which has suffered intensive gravitational flank spreading (van Wyk de Vries et al., 2000), edifice heights are considerably greater for the conical and sub-conical edifices than for the complex massifs (Fig. 11A). The H/W_B ratio clearly separates the three groups (Fig. 11B; 0.16–0.22 for conical edifices; 0.11–0.14 for sub-conical edifices; 0.07–0.09 for complex massifs). The conical edifices have low W_S/W_B ratios (<0.3), whereas the complex massifs have high W_S/W_B ratios (>0.4; not considering Zapatera) and the sub-conical edifices tend to have intermediate values. Ellipticity, irregularity and slopes vary both within and between the edifice types (Fig. 12).

The conical edifices are more circular and regular and have higher slopes, with smooth slope profiles showing constantly increasing slopes up to their small summit regions (Fig. 12). Momotombo is such a cone whose upper flanks have been entirely resurfaced during a 1905 eruption that produced a major lava flow and a large amount of summit-covering scoria, and thus the edifice has a very strong constructional morphology, reflected in its high H/W_B ratio and very low irregularity (Figs. 10 and 12). It is an example of an edifice that is growing faster than the counteracting degradational and structural processes, thus maintaining a regular and steep profile.

The sub-conical edifices have irregular plan shapes and can be either quite circular (Maderas) or very elliptical (Mombacho and Casita), possibly depending on the absence or abundance, respectively, of aligned summit region vents. The slopes of these edifices tend to be less steep than those of conical edifices and also tend to be more variable towards the mid or upper flanks (Fig. 12). Mombacho is notable for its high ellipticity and irregularity (Figs. 10 and 12). This is partly due to three large sector collapses (Shea and van Wyk de Vries, 2008), only one scar of which has been filled in. The other two scars have truncated the summit, and created deep depressions in its flanks (Fig. 10). Its high ellipticity and irregularity are also associated with the presence of multiple summit vents.

The complex massifs are distinguished by their much lower slopes throughout most of their heights (Fig. 12). Rota is strongly eroded, and there are no fresh constructional features on it (Fig. 10). The edifice is cut by a set of north-trending faults that define a central

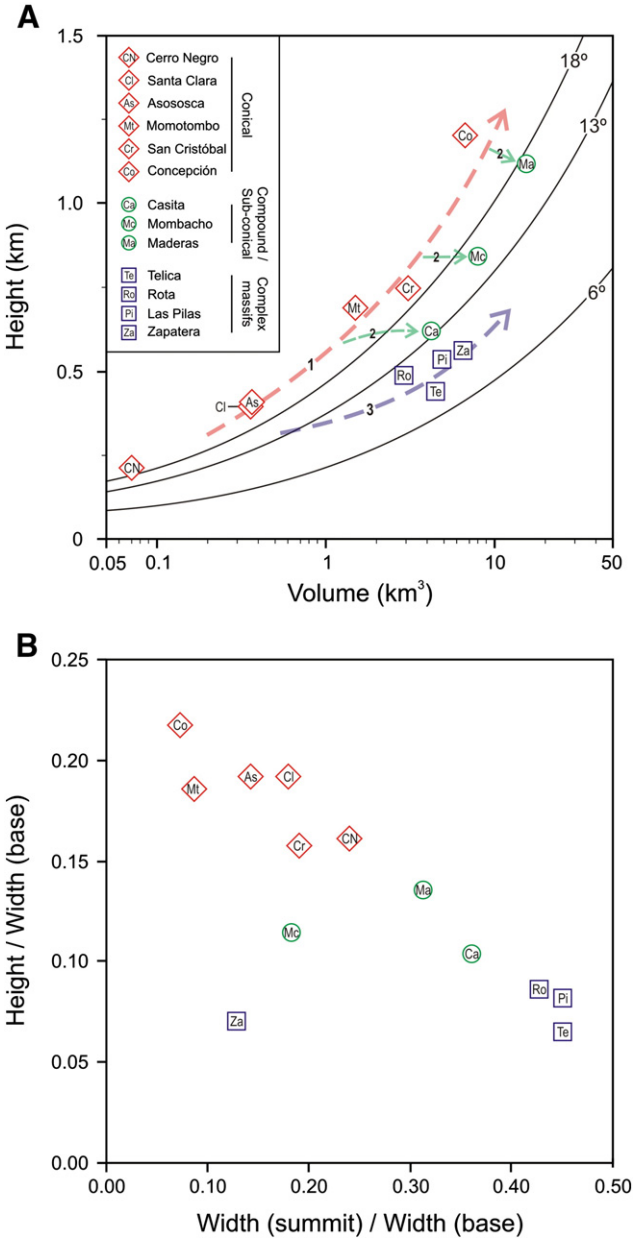

Fig. 11. A) Height vs. volume diagram of Nicaraguan volcanic edifices. Arrows indicate possible growth trends (see text). Curves correspond to slopes of theoretical regular cones, which approximately separate the three edifice types (taken from Grosse et al., 2009). B) Height/width (base) vs. width (summit)/width (base) diagram for the Nicaraguan volcanic edifices.

graben (van Wyk de Vries and Merle, 1998). The volcano is interesting from a morphometric standpoint for the strong tectonic and erosive imprint that can be seen in its high irregularity (Figs. 10 and 12). Rota probably has several summit craters and originally had a more regular shape, but its inactivity has enabled faulting and erosion to degrade it into a small irregular massif.

The Las Pilas complex is a complex massif consisting of an amalgam of several vent systems. The main edifice is a broad summit, lava-dominated shield with a central pit crater. The Las Pilas vent system, located on the northwestern side of the complex, has merged almost completely with the main summit region (Fig. 10). Asososca stands apart at the start of a SSE-trending alignment of several cones, tuff rings and maars (Fig. 10). Cerro Negro and Asososca are arguably part of the Las Pilas complex, but are morphologically distinct from the massif at present (Fig. 10). Cerro Negro has had over ten eruptions since its birth

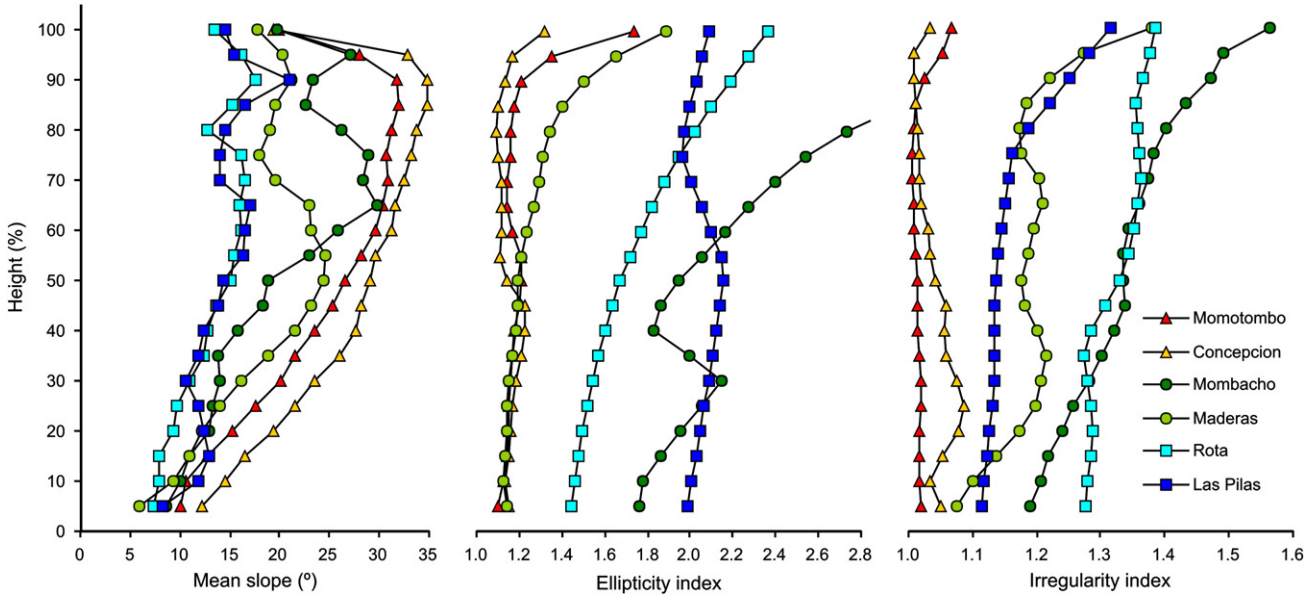

Fig. 12. Mean slope and plan shape (ellipticity and irregularity indexes) plotted as a function of height (%) for six selected Nicaraguan volcanic edifices.

in 1850 and has a conical shape, but vents at its base and on its flank indicate a tendency to evolve towards a more irregular shape even at this early stage. We expect that Cerro Negro will eventually merge with the Las Pilas massif, making a wider, more voluminous, center with no significant height increase. Las Pilas has a relatively low irregularity (e.g., compared to other complex massifs; Fig. 12), probably due to its recent activity; scarce erosional forms are visible.

Different growth trends can be considered for the Nicaragua edifices (Fig. 11A). In locations where there are no structural complications, conical edifices continue growing as cones (arrow '1' in Fig. 11A). In locations with structural complexities (e.g., fault zones), magma supply is disrupted or becomes more diffuse, and conical edifices evolve towards 'sub-conical' edifices (arrows '2' in Fig. 11A), either through vent migration (Casita), or through faulting and collapses, or both (Mombacho). The case of Maderas is different, as it stands on thick lake sediments and has suffered strong gravitational spreading, in this way modifying it from a conical to a 'sub-conical' edifice (van Wyk de Vries and Borgia, 1996). The Nicaraguan complex massifs have too small sizes to derive from the Nicaraguan type conical and 'sub-conical' edifices. They are a separate case of complex volcanic centers which probably become complex massif edifices as soon as they start growing (arrow '3' in Fig. 11A). Cerro Negro, the most recently active center of Las Pilas, illustrates this; since its birth it has already created several satellite vents.

7. Conclusions

DEM datasets with worldwide coverage are now increasingly available, making the morphometric characterization of volcanic edifices at a global scale feasible. Our methodology enables the systematic characterization of most types of volcanic constructs, providing a broad set of quantitative morphometric parameters that thoroughly and objectively describe the size and shape of volcanic edifices. Edifice size is quantified by its basal and summit region dimensions and by its height and volume, plan shape is summarized by the ellipticity and irregularity indexes of elevation contours, and profile shape is described through the H/W_B and W_S/W_B ratios and the average slopes as a function of height.

As shown in Section 5, the parameters will vary in different degrees as a function of DEM source and edifice boundary selection. Our manual boundary delineation method combining curvature and slope data produces average variations of $\pm 3\%$ (and up to $\pm 11\%$) in base area, caused by user subjectivity and the possibility of different break-in-slopes around the edifice. Evidently, a more robust automatic method of boundary delineation is desirable. The size parameters, especially volume, will be the most affected by edifice boundary variability, whereas the H/W_B and W_S/W_B ratios will be less affected. DEM source will also have an effect on these parameters and on the ellipticity and irregularity indexes, slopes and peak count. Variations in height, volume and the H/W_B ratio due to DEM source will be usually smaller than those caused by boundary uncertainty. These parameters will vary mostly by less than $\pm 2.5\%$ ($\pm 1\%$ on average) between the SRTM and ASTER DEMs; the TOPO DEM produces somewhat larger variations mainly because of greater height estimates. The W_S/W_B ratio can vary considerably due to DEM source, specially for edifices with small summit regions. The ellipticity index is least sensitive to DEM source, the irregularity index and peak count are more sensitive, and slope variation is intermediate. The SRTM DEMs produce lower *ei*, *ii*, slope and peak count values because of lower resolution and greater smoothing, whereas errors in the ASTER DEMs will generate higher values. The TOPO DEM is quite rough and generally produces larger *ii* and slope values. However, the *ei*, *ii* and slope vs. height profiles extracted from the different DEM sources generally have similar forms with the same inflections and are thus good records of edifice shape. The SRTM DEM is more adequate for large scale and comparative morphometric studies because it does not have the errors typical of the ASTER G-DEM and its resolution is good enough for composite volcanoes; however, its resolution would be an issue if attempting to study smaller constructs such as scoria cones.

The obtained morphometric parameters are relevant for the investigation of a variety of volcanological processes, as highlighted in the case study of Section 6. Parameters can be used to document and interpret a number of processes associated with morphology and to infer volcanic edifice growth trends. In Nicaragua, conical edifices and complex massifs have distinct morphometric parameters beyond the simple differences previously noted by van Wyk de Vries et al. (2007), clearly showing that the two edifice types are constructed by a different balance of processes. Morphometric analysis gives insights on several of these processes, such as growth vs. erosion rates, gravitational spreading, sector collapse, structural controls and vent migration.

The presented methodology can produce consistent and comparable morphometric datasets that enable to quantitatively document volcano edifice morphologies. Morphometric data can be used both for detailed analysis of a single or a few volcanoes, and for comparisons at a regional or planetary scale. Morphometric datasets enable to investigate in a systematic manner the relations between the constructive and destructive processes acting on volcanoes and their resulting

topographies. Using this methodology, a global morphometric database and classification of volcanic edifices is viable.

Acknowledgments

INETER is thanked for providing the topographic map-derived DEM of Nicaragua. ASTER G-DEM is a product of METI and NASA. PG is grateful to CONICET, Fundación Miguel Lillo and Instituto CEDIAC for their support. MK is supported by the Fonds voor Wetenschappelijk Onderzoek — Vlaanderen. We thank S. Tarquini and an anonymous reviewer, as well as Guest Editor J.-C. Thouret and Chief Editor A. Harvey, for their detailed reviews that helped improve the manuscript.

References

Bleacher, J.E., Greeley, R., 2008. Relating volcano morphometry to the developmental progression of Hawaiian shield volcanoes through slope and hypsometric analyses of SRTM data. Journal of Geophysical Research 113, B09208.
Borgia, A., van Wyk de Vries, B., 2003. The volcanotectonic evolution of Concepción volcano, Nicaragua. Bulletin of Volcanology 65, 248–266.
Borgia, A., Poore, C., Carr, M.J., Melson, W.G., Alvarado, G.E., 1988. Structural, stratigraphic, and petrologic aspects of the Arenal–Chato volcanic system, Costa Rica: evolution of a young stratovolcanic complex. Bulletin of Volcanology 50, 86–105.
Carn, S., 2000. The Lamongan volcanic field, East Java, Indonesia: physical volcanology, historic activity and hazards. Journal of Volcanology and Geothermal Research 95, 81–108.
Carr, M.J., 1984. Symmetrical and segmented variation of physical and geochemical characteristics of the Central American Volcanic Front. Journal of Volcanology and Geothermal Research 20, 231–252.
Carr, M.J., Saginor, I., Alvarado, G.E., Bolge, L.L., Lindsay, F.N., Milidakis, K., Turrin, B.D., Feigeson, M.D., Swisher, C.C., 2007. Element fluxes from the volcanic front of Nicaragua and Costa Rica. Geochemistry, Geophysics, Geosystems 8, Q06001.
Carrara, A., Bitelli, G., Carla, R., 1997. Comparison of techniques for generating digital terrain models from contour lines. International Journal of Geographical Information Science 11, 451–473.
Clague, D.A., Moore, J.G., Reynolds, J.R., 2000. Formation of submarine flat-topped volcanic cones in Hawaii. Bulletin of Volcanology 62, 214–233.
Corazzato, C., Tibaldi, A., 2006. Fracture control on type, morphology and distribution of parasitic volcanic cones: an example from Mt. Etna, Italy. Journal of Volcanology and Geothermal Research 158, 177–194.
Cotton, C.A., 1944. Volcanoes as Landscape Forms. Whitcombe and Tombs Publishing, Christchurch. 416 pp.
Davidson, J., De Silva, S., 2000. Composite volcanoes. In: Sigurdsson, H., Houghton, B., McNutt, S.R., Rymer, H., Stix, J. (Eds.), Encyclopedia of Volcanoes. Academic Press, New York, pp. 663–681.
Davis, J.C., 1986. Statistics and Data Analysis in Geology, Second edition. Wiley, New York. 646 pp.
Dohrenwend, J., Wells, S., Turrin, B., 1986. Degradation of Quaternary cinder cones in the Cima volcanic field, Mojave Desert, California. Geological Society of America Bulletin 97, 421–427.
Dóniz, J., Romero, C., Coello, E., Guillén, C., Sánchez, N., García-Cacho, L., García, A., 2008. Morphological and statistical characterization of recent mafic volcanism on Tenerife (Canary Islands, Spain). Journal of Volcanology and Geothermal Research 173, 185–195.
Duchossois, G., Kohlhammer, G., Martin, P., 1996. Completion of the ERS Tandem Mission. Earth Observation Quarterly 52, 1–2.
Favalli, M., Pareschi, M.T., 2004. Digital elevation model construction from structured topographic data: the DEST algorithm. Journal of Geophysical Research 109, F04004.
Favalli, M., Karátson, D., Mazzuoli, R., Pareschi, M.T., Ventura, G., 2005. Volcanic geomorphology and tectonics of the Aeolian archipelago (Southern Italy) based on integrated DEM data. Bulletin of Volcanology 68, 157–170.
Favalli, M., Karátson, D., Mazzarini, F., Pareschi, M.T., Boschi, E., 2009. Morphometry of scoria cones located on a volcano flank: a case study from Mt. Etna (Italy), based on high-resolution LiDAR data. Journal of Volcanology and Geothermal Research 186, 320–330.
Favalli, M., Fornaciai, A., Mazzarini, F., Harris, A.J.L., Neri, M., Behncke, B., Pareschi, M.T., Tarquini, S., Boschi, E., 2010. Evolution of an active lava flow field using a multitemporal LIDAR acquisition. Journal of Geophysical Research 115, B11203.
Ferretti, A., Monti-Guarnieri, A., Prati, C., Rocca, F., Massonnet, D., 2007. InSAR Principles: Guidelines for SAR Interferometry Processing and Interpretation. ESA Publications, The Netherlands. 246 pp.
Fornaciai, A., Behncke, B., Favalli, M., Neri, M., Tarquini, S., Boschi, E., 2010. Detecting short-term evolution of Etnean scoria cones: a LIDAR-based approach. Bulletin of Volcanology 72, 1209–1222.
Francis, P.W., 1993. Volcanoes: A Planetary Perspective. Oxford University Press, Oxford. 443 pp.
Francis, P.W., Abbott, B.M., 1973. Sizes of conical volcanoes. Nature 244, 22–23.
Grohmann, C.H., Smith, M.J., Riccomini, C., 2011. Multiscale analysis of topographic surface roughness in the Midland Valley, Scotland. IEEE Transactions on Geoscience and Remote Sensing 49, 1200–1213.
Grosse, P., van Wyk de Vries, B., Petrinovic, I.A., Euillades, P.A., Alvarado, G., 2009. Morphometry and evolution of arc volcanoes. Geology 37, 651–654.
Guth, P.L., 1995. Slope and aspect calculations on gridded digital elevation models: examples from a geomorphometric toolbox for personal computers. Zeitschrift für Geomorphologie 101, 31–52.
Hasenaka, T., 1994. Size, distribution, and magma output rate for shield volcanoes of the Michoacán–Guanajuato volcanic field, Central Mexico. Journal of Volcanology and Geothermal Research 63, 13–31.
Hasenaka, T., Carmichael, I., 1985. The cinder cones of Michoacán–Guanajato, central Mexico: their age, volume, distribution and magma discharge rate. Journal of Volcanology and Geothermal Research 25, 104–124.
Hauber, E., Bleacher, J.E., Gwinner, K., Williams, D., Greeley, R., 2009. The topography and morphology of low shields and associated landforms of plains volcanism in the Tharsis region of Mars. Journal of Volcanology and Geothermal Research 185, 69–95.
Hengl, T., Reuter, H.I. (Eds.), 2009. Geomorphometry: Concepts, Software, Applications. Developments in Soil Science, 33. Elsevier, Amsterdam. 765 pp.
Hildreth, W., Fierstein, J., 1997. Recent eruptions of Mount Adams, Washington Cascades, USA. Bulletin of Volcanology 58, 472–490.
Hodgson, M.E., 1998. Comparison of angles from surface slope/aspect algorithms. Cartography and Geographic Information Systems 25, 173–185.
Hone, D.W.E., Mahony, S.H., Sparks, R.S.J., Martin, K.T., 2007. Cladistic analysis applied to the classification of volcanoes. Bulletin of Volcanology 70, 203–220.
Hooper, D., Sheridan, M., 1998. Computer-simulation models of scoria cone degradation. Journal of Volcanology and Geothermal Research 83, 241–267.
Huggel, C., Schneider, D., Miranda, P.J., Delgado Granados, H., Kääb, A., 2008. Evaluation of ASTER and SRTM DEM data for lahar modeling: a case study on lahars from Popocatépetl Volcano, Mexico. Journal of Volcanology and Geothermal Research 170, 99–110.
Jarvis, A., Reuter, H.I., Nelson, A., Guevara, E., 2008. Hole-filled SRTM for the Globe Version 4: CGIAR-CSI SRTM 90 m Database. http://srtm.csi.cgiar.org.
Jones, K.H., 1998. A comparison of algorithms used to compute hill slope as a property of the DEM. Computers and Geosciences 24, 315–324.
Karátson, D., Telbisz, T., Singer, B.S., 2010a. Late-stage volcano geomorphic evolution of the Pleistocene San Francisco Mountain, Arizona (USA), based on high-resolution DEM analysis and $^{40}Ar/^{39}Ar$ chronology. Bulletin of Volcanology 72, 833–846.
Karátson, D., Favalli, M., Tarquini, S., Fornaciai, A., Wörner, G., 2010b. The regular shape of stratovolcanoes: a DEM-based morphometrical approach. Journal of Volcanology and Geothermal Research 193, 171–181.
Kervyn, M., Kervyn, F., Goossens, R., Rowland, S.K., Ernst, G.G.J., 2007. Mapping volcanic terrain using high-resolution and 3D satellite remote sensing. In: Teeuw, R.M. (Ed.), Mapping Hazardous Terrain Using Remote Sensing. Geological Society, London, pp. 5–30.
Kervyn, M., Ernst, G.G.J., Goossens, R., Jacobs, P., 2008. Mapping volcano topography with remote sensing: ASTER vs. SRTM. International Journal of Remote Sensing 29, 6515–6538.
Lagmay, A.M.F., Valdivia, W., 2006. Regional stress influence on the opening direction of crater amphitheaters in Southeast Asian volcanoes. Journal of Volcanology and Geothermal Research 158, 139–150.
Lane, S.N., James, T.D., Crowell, M.D., 2000. The application of digital photogrammetry to complex topography for geomorphological research. The Photogrammetric Record 16, 793–821.
McKnight, S.B., Williams, S.N., 1997. Old cinder cone or young composite volcano? The nature of Cerro Negro, Nicaragua. Geology 25, 339–342.
Michon, L., Saint-Ange, F., 2008. Morphology of Piton de la Fournaise basaltic shield volcano (La Réunion Island): characterization and implication in the volcano evolution. Journal of Geophysical Research 113, B03203.
Mouginis-Mark, P.J., Rowland, S.K., Garbeil, H., 1996. Slopes of western Galapagos volcanoes from airborne interferometric radar. Geophysical Research Letters 23, 3767–3770.
Nelson, A., Reuter, H.I., Gessler, P., 2009. DEM production methods and sources. In: Hengl, T., Reuter, H.I. (Eds.), Geomorphometry: Concepts, Software, Applications. Developments in Soil Science, Elsevier, Amsterdam, pp. 65–85.
Oehler, J.-F., Lénat, J.-F., Labazuy, P., 2007. Growth and collapse of the Reunion Island volcanoes. Bulletin of Volcanology 70, 717–742.
Olaya, V., 2009. Basic land-surface parameters. In: Hengl, T., Reuter, H.I. (Eds.), Geomorphometry: Concepts, Software, Applications. Developments in Soil Science, Elsevier, Amsterdam, pp. 141–169.
Pike, R.J., 1978. Volcanoes on the inner planets: some preliminary comparisons of gross topography. 9th Lunar and Planetary Science Conference, pp. 3239–3273.
Pike, R.J., 1995. Geomorphometry — progress, practice, and prospect. Zeitschrift für Geomorphologie 101, 221–238.
Pike, R.J., Clow, G.D., 1981. Revised classification of terrestrial volcanoes and a catalog of topographic dimensions with new results on edifice volume, U.S. Geological Survey Open-File Report OF 81-1038.
Plescia, J.B., 2004. Morphometric properties of Martian volcanoes. Journal of Geophysical Research 109, E03003.
Poon, J., Fraser, C., Chunsun, Z., Li, Z., Gruen, A., 2005. Quality assessment of digital surface models generated from Ikonos imagery. The Photogrammetric Record 20, 162–171.
Porter, S., 1972. Distribution, morphology, and size frequency of cinder cones on Mauna Kea volcano, Hawaii. Geological Society of America Bulletin 83, 3607–3612.
Rabus, B., Eineder, M., Roth, A., Bamler, R., 2003. The shuttle radar topography mission — a new class of digital elevation models acquired by spaceborne radar. ISPRS Journal of Photogrammetry and Remote Sensing 57, 241–262.
Rappaport, Y., Naar, D.F., Barton, C.C., Liu, Z.J., Hey, R.N., 1997. Morphology and distribution of seamounts surrounding Easter Island. Journal of Geophysical Research 102, 713–728.
Reuter, H.I., Nelson, A., Jarvis, A., 2007. An evaluation of void filling interpolation methods for SRTM data. International Journal of Geographic Information Science 21, 983–1008.
Reuter, H.I., Hengl, T., Gessler, P., Soille, P., 2009a. Preparation of DEMs for geomorphometric analysis. In: Hengl, T., Reuter, H.I. (Eds.), Geomorphometry: Concepts, Software, Applications. Developments in Soil Science, Elsevier, Amsterdam, pp. 87–120.

Reuter, H.I., Nelson, A., Strobl, P., Mehl, W., Jarvis, A., 2009b. A first assessment of ASTER GDEM tiles for absolute accuracy, relative accuracy and terrain parameters. Proceedings 2009 IEEE International Geoscience and Remote Sensing Symposium (IGARSS), 5, pp. 240–243.
Rodríguez, E., Morris, C.S., Belz, J.E., 2006. A global assessment of the SRTM performance. Photogrammetric Engineering and Remote Sensing 72, 249–260.
Rossi, M.J., 1996. Morphology and mechanism of eruption of postglacial shield volcanoes in Iceland. Bulletin of Volcanology 57, 530–540.
Rowland, S.K., Garbeil, H., 2000. Slopes of oceanic volcanoes. In: Mouginis-Mark, P., Crisp, J., Fink, J. (Eds.), Remote Sensing of Active Volcanism: Geophysical Monograph. American Geophysical Union, pp. 223–247.
Schenk, P.M., Wilson, R.R., Davies, A.G., 2004. Shield volcano topography and the rheology of lava flows on Io. Icarus 169, 98–110.
Settle, M., 1979. The structure and emplacement of cinder cone fields. American Journal of Science 279, 1089–1107.
Shan, J., Toth, C.K. (Eds.), 2008. Topographic Laser Ranging and Scanning: Principles and Processing. CRC Press Taylor & Francis Group, London. 590 pp.
Shea, T., van Wyk de Vries, B., 2008. The emplacement of two contrasting debris avalanches at Mombacho Volcano, Nicaragua. Bulletin of Volcanology 70, 899–921.
Simpson, J.F., 1967. The frequency distribution of volcanic crater diameters. Bulletin of Volcanology 30, 335–336.
Smith, D.K., 1988. Shape analysis of Pacific seamounts. Earth and Planetary Science Letters 90, 457–466.
Smith, D.K., 1996. Comparison of shapes and sizes of seafloor volcanoes on Earth and "pancake" domes on Venus. Journal of Volcanology and Geothermal Research 73, 47–64.
Smith, M.J., Clark, C.D., 2005. Methods for the visualization of digital elevation models for landform mapping. Earth Surface Processes and Landforms 30, 885–900.
Smith, D.E., Zuber, M.T., Frey, H.V., Garvin, J.B., Head, J.W., Muhleman, D.O., Pettengill, G.H., Phillips, R.J., Solomon, S.C., Zwally, H.J., Banerdt, W.B., Duxbury, T.C., Golombek, M.P., Lemoine, F.G., Neumann, G.A., Rowlands, D.D., Aharonson, O., Ford, P.G., Ivanov, A.B., Johnson, C.L., McGovern, P.J., Abshire, J.B., Afzal, R.S., Sun, X., 2001. Mars Orbiter Laser Altimeter: experiment summary after the first year of global mapping of Mars. Journal of Geophysical Research 106, 23689–23722.
Stevens, N.F., Manville, V., Heron, D.W., 2002. The sensitivity of a volcanic flow model to digital elevation model accuracy: experiments with digitised map contours and interferometric SAR at Ruapehu and Taranaki volcanoes, New Zealand. Journal of Volcanology and Geothermal Research 119, 89–105.
Stoiber, R.E., Carr, M.J., 1973. Quaternary volcanic and tectonic segmentation of Central America. Bulletin of Volcanology 37, 304–325.
Stretch, R.C., Mitchell, N.C., Portaro, R.A., 2006. A morphometric analysis of the submarine volcanic ridge south-east of Pico Island, Azores. Journal of Volcanology and Geothermal Research 156, 35–54.
Tarquini, S., Isola, I., Favalli, M., Mazzarini, F., Bisson, M., Pareschi, M.T., Boschi, E., 2007. TINITALY/01: a new triangular irregular network of Italy. Annals of Geophysics 50, 407–425.
Thouret, J.C., 1999. Volcanic geomorphology—an overview. Earth-Science Reviews 47, 95–131.
Tibaldi, A., 1995. Morphology of pyroclastic cones and tectonics. Journal of Geophysical Research 100, 24521–24535.
van Wyk de Vries, B., Borgia, A., 1996. The role of basement in volcano deformation. In: McGuire, W.J., Jones, A.P., Neuberg, J. (Eds.), Volcano Instability on the Earth and Other Planets: Geological Society of London Special Publication, 110, pp. 95–110.
van Wyk de Vries, B., Merle, O., 1998. Extension induced by volcanic loading in regional strike-slip zones. Geology 26, 983–986.
van Wyk de Vries, B., Kerle, N., Petley, D., 2000. Sector collapse forming at Casita volcano, Nicaragua. Geology 28, 167–170.
van Wyk de Vries, B., Grosse, P., Alvarado, G.E., 2007. Volcanism and volcanic landforms. In: Bundschuh, J., Alvarado, G.E. (Eds.), Central America: Geology, Resources and Hazards, pp. 123–158. Balkema, Rotterdam.
Ventura, G., Vilardo, G., 2008. Emplacement mechanism of gravity flows inferred from high resolution Lidar data: the 1944 Somma–Vesuvius lava flow (Italy). Geomorphology 95, 223–235.
Wood, C.A., 1978. Morphometric evolution of composite volcanoes. Geophysical Research Letters 5, 437–439.
Wood, C.A., 1980a. Morphometric evolution of cinder cones. Journal of Volcanology and Geothermal Research 7, 387–413.
Wood, C.A., 1980b. Morphometric analysis of cinder cone degradation. Journal of Volcanology and Geothermal Research 8, 137–160.
Wood, J., 1996. The geomorphological characterization of digital elevation models. Ph. D. Thesis. University of Leicester, UK, 185 pp.
Wright, R., Garbeil, H., Baloga, S.M., Mouginis-Mark, P.J., 2006. An assessment of shuttle radar topography mission digital elevation data for studies of volcano morphology. Remote Sensing of Environment 105, 41–53.
Zebker, H.A., Madsen, S.N., Martin, J., Wheeler, K.B., Miller, T., Lou, Y., Alberti, G., Vetrella, S., Cucci, A., 1992. The TOPSAR interferometric radar topographic mapping instrument. IEEE Transactions on Geoscience and Remote Sensing 30, 933–940.
Zuber, M.T., Smith, D.E., Solomon, S.C., Muhleman, D.O., Head, J.W., Garvin, J.B., Abshire, J.B., Bufton, J.L., 1992. The Mars Observer Laser Altimeter investigation. Journal of Geophysical Research 97, 7781–7797.